Response to the comments from GPIRB committee

RE: Manuscript Number 25-M-09GP, entitled "ISOCAPES as a Regional-Scale Tool for Understanding Groundwater Uranium Cycling in the Pine Ridge Reservation, South Dakota."

Dear committee members, May 21th, 2025

We would like to thank you for reviewing our manuscript. We have revised the comments and addressed the comments mentioned in your previous communication.

Comments from GPIRB are marked in black and bold font, our response is in blue:

1. **Line 37 is blank, and Line 38 indicates "working on it-will finalize before submission"**

Addressed. We have included the TOC art in Line 16-17.

2. **In the Supplementary Information, S3 - information is pending**

Addressed. We have incorporated the missing information in the revised version. (Line 50-63 in the supplementary section)

3. Figure S1 - comment box indicates the information needs to be double checked

Addressed and we have removed any leftover comments in the revised version after addressing the comment. (updated Fig S1)

We hope that after these revisions the manuscript will be approved by Great Plains Institutional Review Board for submission in Environmental Science and Technology journal for publication.

Best regards,

Arijeet Mitra

Post doctoral Researcher
Columbia University Northern Plains Superfund Program

Lay summary:

Native American communities in the Northern Plains often rely on private wells for drinking water, but the water from many of these wells contain uranium, sometimes above the EPA's safe limit. This study looks at how uranium spreads in groundwater in the Pine Ridge Reservation (PRR) in South Dakota by testing water samples from private wells. We analyzed 140 groundwater samples for uranium levels, uranium isotope ratios, and elements that indicate chemical conditions, such as iron, manganese, nitrate, sulfate, selenium, and vanadium. Uranium levels ranged from less than 1 to 48 micrograms per liter (μg/L), with 5% of the samples exceeding the EPA's safe limit of 30 μg/L. How uranium moves in groundwater depends on oxygen levels. With more oxygen, it dissolves and flows with the water. When there is no oxygen, it can form solid particles and naturally settle out. The proportion of uranium isotopes in groundwater works like a fingerprint. It helps us track where uranium enters and leaves the water and whether it comes from nearby or far away. Using this fingerprint, we found that in the northeastern part of the Reservation, oxygen-rich conditions break down minerals, releasing high amounts of uranium (28-45 μg/L). In contrast, in the southwest, chemical reactions remove uranium from the water, leading to lower uranium levels. Further analysis identified four types of groundwater environments, showing how water chemistry affects uranium levels in water. These findings show that tracking uranium isotopes and water chemistry helps us understand how uranium spreads. By tracking uranium's chemical signature, we can see how contamination hotspots change over time. This study helps PRR communities find safe drinking water and plan ways to reduce contamination. Protecting groundwater is key to reducing uranium exposure and keeping communities safe.

ISOSCAPES as a Regional-Scale Tool for Understanding Groundwater Uranium Cycling in the Northern Plains

Authors: *Arijeet Mitra[1], Randall Hughes[2], Tracy Zacher[2], Rae O'Leary[2], Bayley Sbardellati[3], Mason Stahl[3], Reno Red Cloud[4], Shams Azad[5], James Ross[5], Ben Bostick[5], Steve Chillrud[5], Alex N. Halliday[5], Ana Navas-Acien[1], Kathrin Schilling[1], Anirban Basu[1]*

Author details: [1]Mailman School of Public Health, Columbia University, New York, NY 10032, [2]Missouri Breaks Industries Research Inc, Eagle Butte, SD 57625, [3]Environmental Science Policy and Engineering, Union College, 807 Union Street, Schenectady, NY 12308, [4]Oglala Sioux Tribe Water Resources, Pine Ridge, SD 57770, [5]Lamont Doherty Earth Observatory, Columbia University, 61 Route 9W, Palisades, NY 10964

***Corresponding address:** am6368@cumc.columbia.edu

Target journal: Environmental Science and Technology

16 **TOC Art**

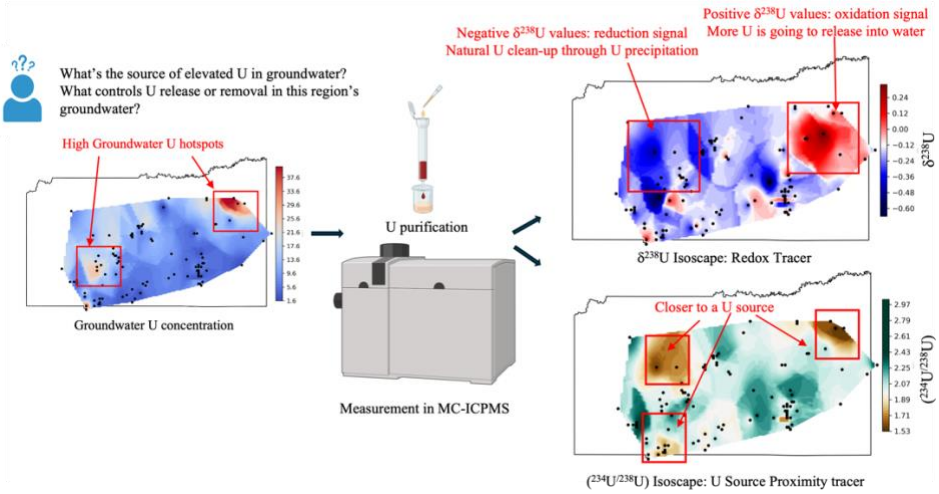
What's the source of elevated U in groundwater?
What controls U release or removal in this region's groundwater?
High Groundwater U hotspots
Groundwater U concentration
U purification
Measurement in MC-ICPMS
Negative δ238U values: reduction signal
Natural U clean-up through U precipitation
Positive δ238U values: oxidation signal
More U is going to release into water
δ238U Isoscape: Redox Tracer
Closer to a U source
(234U/238U) Isoscape: U Source Proximity tracer

17

ABSTRACT

Groundwater uranium (U) contamination poses a significant health risk, particularly in Native American communities reliant on private wells. This study examines groundwater U cycling in a tribal region in South Dakota participating in the Strong Heart Water Study, by analyzing samples from private wells of local communities. The groundwater samples (n=140) were analyzed for U concentrations, $\delta^{238}U$, ($^{234}U/^{238}U$) activity ratios, and redox-sensitive elements including iron (Fe), manganese (Mn), nitrate (NO_3^-), sulfate (SO_4^{2-}), selenium (Se), and vanadium (V). Uranium concentrations range from 0.40 to 48.25 µg/L, with 5% exceeding the USEPA maximum contaminant level of 30 µg/L. Spatial patterns in $\delta^{238}U$ and ($^{234}U/^{238}U$) reveal distinct U mobilization processes. Oxidative dissolution in the northeast of the study area leads to elevated U concentrations (28-45 µg/L) and higher $\delta^{238}U$ values (-0.08 to 0.3 ‰), while U reducing conditions in the southwest promote U removal through reduction reflected in lower $\delta^{238}U$ values (-0.61 to -0.30 ‰). Cluster and principal component analyses identify four distinct groundwater environments, highlighting how redox heterogeneity governs U transport and retention. This study highlights the value of integrating U isotope compositions with redox indicators and statistical analysis to characterize subsurface U cycling. Understanding these processes is crucial for groundwater management and mitigation strategies in U-impacted regions.

HIGHLIGHT

Isotopic and statistical analyses identify groundwater U release and retention zones, providing insights into contamination risks and mitigation strategies in a tribal region in South Dakota participating in the Strong Heart Water Study.

KEYWORDS

Groundwater; Isoscapes; U isotopes; U activity ratios; Redox; Native American Communities

INTRODUCTION

Safe drinking water is a critical concern in Native American communities due to limited infrastructure and widespread groundwater contamination.[1,2] Approximately 6.5% of Native American households lack access to safe and adequate water sources or waste disposal facilities, compared to less than 1% of households in the general U.S. population.[3,4] Additionally, groundwater contamination from uranium (U) and arsenic (As) poses serious health risks, especially in Native American communities relying on private, unregulated wells[2,5–9]. Communities participating in the Strong Heart Water study (SHWS), located in the Northern Plains, have reported groundwater U concentrations as high as 60 ppb—nearly double the United States Environmental Protection Agency's (USEPA) maximum contaminant level (MCL) of 30 ppb.[10,11] Public health studies have shown that residents in these areas experience a 40% higher cancer mortality rate than the national average[12] and have the highest documented U and As exposure among all demographic groups in the U.S.[13,14]

While legacy uranium mining in parts of South Dakota has raised concerns about mining-related contamination, [15–19, 18,19]there are currently no legacy or active U mines within or near SHWS study sites. Instead, elevated groundwater U concentrations in this region are primarily attributed to geogenic sources, as mineralized zones are dispersed throughout the subsurface. [19] The dissolution of U-bearing bedrock results in non-point source contamination in aquifers, particularly in areas where residents rely on untreated private wells for drinking, livestock, and irrigation. Despite ongoing infrastructure improvements, many households in these communities remain dependent on private wells, increasing their vulnerability to naturally occurring contaminants. Understanding the processes that governs the release or removal of U in groundwater is essential for identifying high-risk areas and developing effective mitigation strategies.

While dissolved U concentrations provide a general indication of U contamination, they alone are insufficient to characterize the geochemical processes that control U mobility in groundwater. A key factor influencing U solubility in groundwater is its oxidation state. Under reducing conditions and near-neutral pH, the highly soluble oxidized U(VI) undergoes reduction to insoluble U(IV), leading to the formation of U-containing solids, such as uraninite, which are effectively immobilized. This reduction is primarily driven

by microbially mediated terminal electron-accepting processes in aquifers, such as iron (Fe (III)) reduction and/or sulfate (SO_4^{2-}) reduction.[20–26] However, reduced U(IV) solids are susceptible to reoxidation and easily oxidized by dissolved oxygen or nitrate to form soluble U(VI).[27,28] The presence of complexing agents like bicarbonate and organic ligands stabilizes dissolved U(VI) in groundwater and enhances its mobility. Therefore, local variations in aquifer geochemistry, mineral composition, organic matter content, and microbial activity create heterogeneous redox zones, further complicating the interpretation of the spatial distribution of dissolved U in groundwater. This challenge can be addressed by using indicators sensitive only to the U redox reactions. Fractionation of U isotopes (i.e. changes in $^{238}U/^{235}U$) serve as indicator of environments conducive to U(VI) reduction and mobilization (Table S1).[29–32]

Uranium isotope fractionation occurs due to the nuclear volume effect (NVE), which results from differences in nuclear size rather than mass between isotopes.[33–35] Because ^{238}U has a disproportionately larger nuclear volume than ^{235}U and therefore a lower electron density at the nucleus, it is preferentially incorporated into reduced U(IV) phases during reduction, resulting in lower overall energy and a more thermodynamically stable configuration. Consequently, U(VI) remaining in solution becomes progressively enriched in ^{235}U. This isotopic fractionation is expressed as ε (epsilon), representing the per mil (‰) deviation of the isotopic ratio between U(IV) and U(VI), and is calculated as $\varepsilon = 1000 \times (\alpha - 1)$, where α (alpha) is the isotopic fractionation factor defined as $[(^{238}U/^{235}U)_{U(IV)}/(^{238}U/^{235}U)_{U(VI)}]$. Laboratory experiments have demonstrated that U isotope fractionation (as ε) during microbial U(VI) reduction can reach approximately 1‰,[36,37] while abiotic reduction by FeS, a product of microbial sulfate reduction, results in similar fractionation (~0.8‰).[29] This consistency underpins the reliability of U isotope ratios as reliable indicators of reduction, regardless of whether the process is biologically or chemically mediated. In contrast, U(VI) removal by adsorption on to mineral surfaces leads to minimal fractionation ($\varepsilon \sim -0.2$‰), with a slight preference for ^{235}U adsorption, producing an effect opposite to that of reduction-driven fractionation.[38,39]

Variation in U activity ratios or ($^{234}U/^{238}U$) in groundwater may serve as an effective indicator for assessing U source proximity and transport (Fig S1). In U-enriched sandstone-type deposits, ($^{234}U/^{238}U$) approaches secular equilibrium over geological timescales, as the decay of ^{238}U is balanced by the ingrowth of ^{234}U, resulting in a ratio near unity. In closed systems, this equilibrium is generally established within approximately one million years. However, in natural systems, this equilibrium is often disrupted by water-rock interactions that preferentially mobilize ^{234}U. Such disequilibrium arises from α-recoil, in which recoil energy from the decay of ^{238}U displaces its daughter nuclide ^{234}U by approximately 20–30 nanometers in silicate minerals. As a result, some of these atoms are relocated toward grain boundaries or microfractures, where they are more susceptible to leaching.[40,41] The extent of ^{234}U recoil loss is influenced by the grain size and geometry of U-bearing minerals and tends to increase as grain size decreases.[42–44] This process can lead to ($^{234}U/^{238}U$) values below 1 in U-bearing minerals, while surrounding groundwater becomes enriched in ^{234}U, with ratios exceeding 1. Importantly, U transport in groundwater directly influences ($^{234}U/^{238}U$) values. When dissolved U stays close to its source, groundwater ($^{234}U/^{238}U$) reflects the U activity ratio of the source and is maintained near secular equilibrium. In contrast, when U is transported over longer distances without precipitation, continued α-decay in groundwater and sustained ^{234}U release from minerals along the flow path led to progressively elevated ($^{234}U/^{238}U$) values in groundwater. For instance, groundwater in contact with sandstone-hosted U ores often exhibits ($^{234}U/^{238}U$) values like those of the ore, indicating a dominant influence from the local source.[45] However, as U migrates farther from its source, prolonged interaction with aquifer materials and continual ^{234}U production elevate ($^{234}U/^{238}U$), signaling longer transport distances and cumulative effects of recoil-driven fractionation.[45] Overall, U activity ratios in groundwater serve as sensitive tracers for distinguishing between local and distal U sources and offer mechanistic insights into U mobility in the subsurface.

In this study, we report U concentration, $^{238}U/^{235}U$, ($^{234}U/^{238}U$), and additional redox-sensitive indicators such as nitrate (NO_3^-), iron (Fe), manganese (Mn), selenium (Se), vanadium (V) and sulfate (SO_4^{2-}) in groundwater samples collected from private wells from a tribal land in the Northern Plains. We

integrate these geochemical data with field parameters—temperature, pH, redox potential (Eh), and electrical conductivity (EC) — to perform cluster and principal component analyses (PCA), that allows us to determine of spatial redox variability in groundwater. By incorporating multiple geochemical proxies, our work provides a comprehensive framework for understanding groundwater U cycling in aquifers underlying this tribal land.

MATERIAL AND METHODS

Study Population: This study was conducted as part of a community-engaged effort in collaboration with Native American communities in the Northern Plains, within the framework of the Strong Heart Water Study (SHWS).[46–52] All research activities including participant recruitment, informed consent, and data collection—were carried out in partnership with Missouri Breaks Industries Research, Inc. (MBIRI), a Native American owned medical research organization. MBIRI facilitated community engagement and implementation through established networks of tribal leaders, and local institutions. The study was approved by appropriate Tribal Research Review Boards, and all activities adhered to principles of ethical research conduct and tribal data sovereignty. In accordance with data sovereignty principles, participating tribes retain ownership of the data, exercise decision-making authority over its future use, and are actively involved in guiding how findings are interpreted and disseminated. To uphold these commitments and protect confidentiality, the identities of participating communities and precise sampling locations are not disclosed. Household recruitment was conducted through community outreach led by MBIRI, and groundwater samples were collected only after informed consent was obtained. Participants had the opportunity to receive their household water quality results and were informed about any contaminants exceeding health-based guidelines. This participatory model ensures that research activities are responsive to community priorities and supports culturally respectful engagement throughout the study lifecycle.

Study area: The study area spans approximately 9,000 km² of a tribal land in southwestern South Dakota and is located southeast of the Black Hills. The region is underlain by sedimentary formations of the White River Group and the Arikaree Formation (Figure S2-3). The Arikaree Formation, the primary aquifer in this area, is composed of fine- to medium-grained sandstone, siltstone, and volcanic ash layers.[53] The basal

sandstone units of the White River Group contain ore-grade U mineralization in the form of roll-front deposits.[54] These deposits, often hosted within paleochannel systems, are known to contribute to localized U enrichment in groundwater.[55] The Arikaree aquifer is predominantly unconfined, and groundwater generally flows from south to north (Fig 1).[56] Due to the structural flatness of the formation—with a regional dip of less than one degree—the potentiometric surface is primarily influenced by topography and the local drainage network.[57] The depth to the water table ranges from approximately 45 to 84 meters in upland areas, to as shallow as 0 to 15 meters in stream valleys and low-lying regions.[56] Rain and spring snowmelt recharge the aquifer and drive seasonal changes in groundwater levels.

Sampling approach: Groundwater samples were collected from 140 private wells across the study area as part of a community-based monitoring initiative. Sampling locations were selected based on participant household locations and reflect a non-random, human-centered sampling design. Field measurements—including pH, redox potential (Eh), and electrical conductivity (EC)—were recorded in situ during sampling. Groundwater samples were analyzed for U concentration, isotopic ratios ($^{238}U/^{235}U$ and $^{234}U/^{238}U$), and other redox-sensitive parameters such as nitrate (NO_3^-), iron (Fe), manganese (Mn), selenium (Se), vanadium (V), and sulfate (SO_4^{2-}). Additional methodological details, including sampling protocols, analytical techniques, and quality assurance procedures, are provided in the Supporting Information (Sections S1–S3).

ISOTOPIC ANALYSIS

The $^{235}U/^{238}U$ measurements in groundwater were carried out using a Nu Plasma 3 MC-ICP-MS (Wrexham, UK) operating in low-resolution mode at the Novel Isotopes in Climate Environment and Rocks (NICER) lab, Lamont-Doherty Earth Observatory, Columbia University using a double-spike technique described in references.[31,58–60] All samples were purified using the UTEVA resin (Eichrom) prior to isotopic measurements (Details in SI: S4). During isotopic analysis, the $^{233}U/^{236}U$, $^{234}U/^{236}U$, $^{235}U/^{236}U$, $^{234}U/^{238}U$, and $^{238}U/^{236}U$ ratios were simultaneously measured. The $^{238}U/^{235}U$ ratios are reported as $\delta^{238}U$, defined by:

$$\delta^{238}U\ (‰) = \left[\frac{\frac{^{238}U}{^{235}U_{sample}}}{\frac{^{238}U}{^{235}U_{CRM145}}} - 1\right] \times 1000 \qquad \text{(eq. 1)}$$

The analytical uncertainty of $\delta^{238}U$ measurements, determined as twice root mean square difference for 19 pairs of duplicate sample preparations (15% of the total samples), is 0.08‰. The ($^{234}U/^{238}U$) were determined from measured $^{234}U/^{238}U$ using CRM 145 as the bracketing standard (($^{234}U/^{238}U$) =0.963). The analytical precision (2σ) of the ($^{234}U/^{238}U$) measurements is 0.01.

GEOSPATIAL ANALYSIS

A spatial interpolation approach was implemented to visualize the geospatial distribution of groundwater U concentration, $\delta^{238}U$, and ($^{234}U/^{238}U$) across the study area. Given the irregular distribution of groundwater sampling locations**,** Inverse Distance Weighting (IDW) interpolation[61] was used to estimate the spatial variation of these parameters. IDW was selected over other commonly used methods—including ordinary kriging (Gaussian and spherical models), cokriging, natural neighbor, and spline interpolation—due to its robustness in settings with limited and unevenly distributed data, where assumptions of stationarity or strong spatial autocorrelation required by geostatistical methods may not be valid. [62–66] Kriging methods are statistically robust but rely on variogram modeling, which can introduce uncertainty when data are limited, or spatial patterns are unclear. Other techniques like cokriging, natural neighbor, and spline interpolation may also perform poorly in sparsely sampled or geochemically complex areas, often resulting in unrealistic gradients or edge effects. In contrast, IDW emphasizes spatial proximity without relying on modeled trends, making it useful for visualizing localized geochemical variability in fractured aquifer systems; however, its assumption of smooth distance decay may oversimplify anisotropic flow and complex heterogeneity, limiting its accuracy in detailed hydrogeologic analysis. However, a key limitation of IDW is that it does not provide estimates of prediction uncertainty or spatial error variance, in contrast to kriging methods that quantify interpolation confidence through modeled variograms. Given that our primary aim was to visualize geospatial trends in redox chemistry rather than quantify interpolation precision, we consider this trade-off acceptable. The study area boundary was defined using a geospatial shapefile,

ensuring spatial accuracy. Sample locations were converted into a GeoDataFrame, and a Delaunay triangulation-based convex hull mask[67] was generated to restrict interpolation within the sampled region, reducing the impact of extrapolation beyond the known dataset. A 100 × 100 mesh grid (~1.73 km × 0.92 km) was created to provide a fine-scale spatial resolution for the interpolated values. The IDW interpolation was applied using the five nearest neighbor sample points, balancing local precision while minimizing overfitting effects. The interpolated values were then visualized as contour maps, with masked regions outside the convex hull removed to maintain interpolation integrity. Sample locations were overlaid on the maps, and the study area boundary was delineated to provide geographical context (Figure 1-3). To further analyze the spatial characteristics of groundwater chemistry, clusters identified from the K-means clustering analysis (see the following section) were plotted on the interpolated maps using distinct marker symbols (Figure 3). This visualization allowed for the examination of how different clusters are distributed spatially across the study area, offering additional insights into spatial patterns of geochemical variability and U transport mechanisms. These geospatial representations provide a comprehensive framework for identifying contamination hotspots, complementing the statistical clustering and multivariate analyses discussed in following sections.

CLUSTER ANALYSIS

Unsupervised clustering techniques, including K-means and hierarchical clustering, were employed to classify groundwater samples based on geochemical characteristics. Numerical variables—including U concentration, $\delta^{238}U$, ($^{234}U/^{238}U$), redox-sensitive indicators (e.g., Fe, Mn, Se, V, As, NO_3^-, SO_4^{2-}), F^-, Cl^-, and field parameters (pH, Eh, EC)—were standardized via z-score normalization to ensure comparability across different scales. The optimal number of clusters (k) was determined using the Elbow Method [68] and Silhouette Score [69] (see SI, Figure S4), ensuring well-separated, internally cohesive groupings. Hierarchical clustering (Ward's method) validated the robustness of the clustering results, and a dendrogram based on Euclidean distance illustrated sample similarity (Figure 4). [70] Box plots were used to compare geochemical differences between clusters, providing insights into U mobility and redox-driven

variability (See SI, Figure S11-14). Additional methodological details are provided in Supplementary Information (SI), Section S5.

PRINCIPAL COMPONENT ANALYSIS (PCA)

PCA was employed to reduce dataset dimensionality and identify dominant geochemical trends. Standardized variables were projected onto principal components (PCs), and the explained variance ratio was analyzed. The first two PCs accounted for ~28% of dataset variance, justifying dimensionality reduction (Figure 5). PCA scores were visualized, with sample clusters differentiated in PC space. A biplot illustrated variable loadings, highlighting geochemical drivers of U mobility. These findings complemented the cluster analysis, offering an integrated perspective on groundwater chemistry. [71–73] Further details on PCA implementation and loadings are included in SI, Section S6.

RESULTS AND DISCUSSION

Geochemistry and isotope geochemistry of groundwater: The concentrations of trace elements, NO_3^-, SO_4^{2-}, fluoride (F^-) and chloride (Cl^-) along with the field parameters for the groundwater samples are presented in Table S2. The pH of the groundwater samples ranges from 6.2 to 8.5, with a median value of 7.6. The EC varies between 190 and 927 µS/cm, with a median value of 431 µS/cm. Fluoride (F^-) and chloride (Cl^-) concentrations, with median values of 0.3 mg/L and 4.3 mg/L, respectively, remain below the EPA Maximum Contaminant Level (MCL) limits of 4 mg/L for F^- and 250 mg/L for Cl^-, indicating no widespread contamination from these anions. Dissolved U (or U(VI)) ranges from 0.4 to 48.25 µg/L (median: 7.5 µg/L; Table S3), with 5% of samples exceeding the USEPA MCL of 30 µg/L**.** High-U samples are predominantly located in the northeastern and southwestern sections of the Arikaree aquifer (Figure 1), where the depth to water is relatively shallow compared to the rest of the aquifer. [56] In these areas, thinning of the Arikaree aquifer brings the White River Group, which hosts ore-grade U in roll-front deposits within the basal Chadron Formation, closer to the surface (Fig S2-3).[54] A few isolated occurrences of elevated U concentrations are observed across the study area, reflecting the heterogeneous distribution of U within the aquifer (Fig. 1).

Groundwater $\delta^{238}U$ values provide key insights into the processes that control the release and removal of groundwater U in this region (Table S3). The $\delta^{238}U$ values range from -1.06‰ to 0.9‰, displaying a variation of up to 2 ‰ (Fig. 2a). Only 6% of the samples exhibit $\delta^{238}U$ values > 0.10‰, while the majority (93%) fall within 0.10‰ to -0.6‰, with a median of -0.19‰ (Fig S6). One sample with a large negative $\delta^{238}U$ value (-1.06‰) is located at the western boundary of the convex hull, where it is excluded from the isoscape due to spatial constraints but not from statistical analysis. The $\delta^{238}U$ isoscape (Fig. 2a) reveals a regional trend, with higher $\delta^{238}U$ values in the northeastern region of the study area and lower values in the southwestern region. Notably, both regions show high-U concentrations in groundwater (Fig 1). The confidence in spatial interpolation of U concentrations and $\delta^{238}U$ variability is assessed using semi variograms (SI, Fig. S6). The semi variogram for U concentration shows that values remain spatially correlated up to 80 km, indicating a broad regional trend. In contrast, $\delta^{238}U$ exhibits strong variability at much smaller scales, with most changes occurring over distances of less than ~10-20 km. This suggests that $\delta^{238}U$ is primarily influenced by localized redox conditions and small-scale hydrogeochemical heterogeneity, rather than large-scale regional trends. However, the presence of small-scale mineralized zones (100-meter or less), typically found in sandstone-hosted U deposits, introduces uncertainty in the semi variogram predictions. Sparse and unevenly distributed private wells—tied to variations in population density— further limits the resolution of regional U cycling trends.[74] Despite these challenges, our spatial dataset provides the best available regional scale understanding of U mobility in this aquifer system.

To account for the observed U isotopic fractionation in the groundwater samples, we evaluated the role of key redox processes. These include oxidative dissolution of source rocks, localized U(VI) reduction, and mixing between reduced groundwater and oxidized recharge water, which can alter U isotopic signatures depending on the extent of redox interactions during mixing. A density plot of compiled $\delta^{238}U$ values from sandstone-hosted U [75–77], which represent the dominant U source in this region, is shown in Fig. S7. It exhibits a range of -0.26‰ to 0.84‰, with a median of 0.33‰. Groundwater samples with positive $\delta^{238}U$ values from 0.10 ‰to 0.80 ‰ closely match the $\delta^{238}U$ signature of the source rock. This suggest that their U isotopic composition is primarily derived from oxidative dissolution of U-bearing rocks

present in the aquifer, a process that causes negligible isotope fractionation and preserves the original source signature[78]. However, the majority **(**93%**)** of groundwater samples with $\delta^{238}U$ value ranging from -1.06‰ to 0.10‰, deviates from the expected oxidative dissolution baseline (~0.33‰). This systematic decrease in $\delta^{238}U$ provides strong evidence for U reduction occurring throughout the dataset, with the extent of reduction varying among samples. Even the least fractionated samples ($\delta^{238}U$ = 0.1‰) suggest partial U(VI) reduction, while the most fractionated waters ($\delta^{238}U$= –1.06‰) indicate more extensive reduction. The magnitude of observed fractionation in most samples, while significant, appears to be muted compared to the stronger fractionation observed in well-mixed experimental systems.[37] This pattern suggests that U(VI) reduction may be taking place in diffusion-limited microenvironments, such as organic rich zones or fine-grained sediments, with low permeability. In these isolated systems, reduced U(IV) becomes sequestered and has restricted exchanges with the surrounding U(VI) pool, as most groundwater flow and dissolved U bypass these zones. In these isolated zones, which are connected to the bulk groundwater primarily through diffusion, restricted transport of U(VI) to reduction sites weakens isotopic fractionation in the surrounding groundwater, leading to a dampened $\delta^{238}U$ signal. A similar process has been observed for selenium[79] and chromium[80] isotope systems, where diffusion limitation within isolated reducing sediments weakens the isotopic fractionation observed in dissolved Se or Cr. Additionally, the spatial distribution of $\delta^{238}U$ observed in the groundwater samples indicates that U reduction occurs in localized redox pockets rather than uniformly throughout the aquifer.

Uranium adsorption onto mineral surfaces is likely a minor contributor to the observed $\delta^{238}U$ variation, given the high Ca concentrations (4 to 346 mg/L with median value at 45 mg/L) in these groundwater samples. Experimental studies [81–83] have demonstrated that when Ca concentrations exceed ~40 mg/L, the dominant aqueous U(VI) species is the neutrally charged calcium-uranyl tri-carbonate complex, $Ca_2UO_2(CO_3)_3^0(aq)$, comprising over 90% of total dissolved U(VI). Our U speciation calculations confirm that over 95% of the U in our groundwater samples exists as $Ca_2UO_2(CO_3)_3^0(aq)$ (Table S4). Because this neutrally charged U species has low affinity for mineral surfaces, adsorption likely plays only

a minor role in the observed isotopic fractionation. However, despite the predominance of neutral U species, adsorption-induced isotopic fractionation cannot be entirely ruled out. Variations in geochemical conditions may still cause slight ^{235}U enrichment in some samples, producing an isotopic signature in the opposite direction of that caused by reduction.

The spatial distribution of additional redox-sensitive indicators, including nitrate (NO_3^-), dissolved Mn, Fe, Se, and V concentrations (SI, Table S1), is consistent with the reducing environments identified from $\delta^{238}U$ data. In groundwater, microbial metabolism generally progresses from NO_3^- reduction to Mn (IV) and Fe (III) reduction, depending on the availability of electron acceptors. In the western portion of the aquifer, low NO_3^- and elevated Fe and Mn concentrations (Fig. 3) indicate that reducing conditions have progressed to Fe(III) and Mn(IV) reduction. Most groundwater samples (92%) contain NO_3^- below the USEPA MCL of 10 mg/L, a pattern that is consistent with the progression of reducing conditions beyond nitrate reduction. Isolated samples with elevated NO_3^- levels above MCL of 10 mg/L likely reflect anthropogenic sources such as agricultural runoff or wastewater infiltration. The absence of a correlation between NO_3^- and $\delta^{238}U$ values (SI, Fig. S8) suggests that nitrate is not a primary oxidant driving U mobilization in this system. Dissolved Mn and Fe concentrations range from 0.03 to 752 µg/L (median: 143 µg/L) and 0.1 to 997 µg/L (median: 23 µg/L), respectively. Although Mn and Fe concentrations do not show a strong direct correlation with $\delta^{238}U$, a clear redox-dependent pattern is observed. Lower $\delta^{238}U$ values (-0.14‰ to -0.50‰, median: -0.23‰) correspond to higher Mn (228–997 µg/L, median: 501 µg/L) and Fe (24–752 µg/L, median: 28 µg/L) concentrations, consistent with Mn (IV) reduction and Fe (III) reduction. Conversely, higher $\delta^{238}U$ values (0.33‰ to 0.16‰) are associated with lower Mn (0.03–41.35 µg/L, median: 0.41 µg/L) and Fe (0.6–13.56 µg/L, median: 1.10 µg/L) concentrations (Figure. 3). These trends provide further support for the presence of U-reducing conditions in the southwestern part of the aquifer, consistent with inferences based on $\delta^{238}U$ patterns. Additionally, spatial distribution of Se and V follows the redox pattern established by $\delta^{238}U$ data (SI, Fig. S9). Higher Se and V concentrations are observed in the northern section, where oxidizing conditions dominate, while lower Se and V concentrations are found

in the southwestern section, where reducing conditions prevail. This observation is in line with the known behavior of redox-sensitive elements Se and V, which become less soluble under reducing conditions.

Arsenic in the study area is mobilized under non-reducing conditions, likely through mechanisms other than reductive dissolution. Dissolved As concentrations range from 0.02 to 24.82 µg/L (median: 5.19 µg/L; Table S1), with 22% of samples exceeding the USEPA MCL of 15 µg/L (Fig S8). The central and northeastern parts of the study area exhibit elevated As concentrations (Fig. S8). Elevated As concentrations are observed in areas where Fe and Mn levels are low and $\delta^{238}U$ values indicate oxic to suboxic groundwater. These observations suggest that As is being released through processes other than the reductive dissolution of Fe oxides. Notably, groundwater in these parts of the aquifer contains elevated Na concentrations, with a median of 53 mg/L (range: 3–660 mg/L. High Na levels can inhibit As(V) adsorption onto Fe–Al oxides via the counterion effect, in which Na^+ reduces the positive surface charge of mineral surfaces and weakens the electrostatic attraction to negatively charged arsenate species.[84,85] This mechanism may contribute to elevated As concentrations under oxidizing, Na-rich conditions in the region, consistent with observations from other aquifer systems.[86–88]

Variation of U activity ratio or ($^{234}U/^{238}U$) in groundwater: The ($^{234}U/^{238}U$) of groundwater provide insights into U source proximity, redox conditions, and groundwater residence time within the Arikaree aquifer. The ($^{234}U/^{238}U$) in groundwater samples range from 1.53 to 3.07, with a median value of 2.03 (SI, Table S2, Fig. 2b). Most samples (85%) fall within narrower range of 1.8 to 2.5, while 15% of samples exhibit ($^{234}U/^{238}U$) values between 1.53 to 1.8 (Fig S10). These variations reflect combined influences of geological setting, rock–water interactions, redox processes, and alpha recoil. In this region, U occurs in heterogeneously distributed mineralized zones within the host rock, which exhibit $^{234}U/^{238}U$ activity ratios ranging from 0.6 to 1.6, with a median of 1.0 (Fig SI, S10).[31,89–91]

Groundwater samples with low ($^{234}U/^{238}U$) values (1.53–1.8) are concentrated in the northern and southwestern parts of the aquifer, where the Arikaree formation is thinner and the underlying White River Group host to ore-grade U deposits[54] lies closer to the surface (Fig S2-3). In these areas, USGS test wells have intersected the White River Group at shallower depths (27–72 meters), compared to deeper

penetrations (91–252 meters) elsewhere in the aquifer. [92] Within these U-bearing deposits, the alpha decay of ^{238}U over geological timescales causes ^{234}U atoms to migrate toward mineral grain boundaries via alpha recoil. Subsequent interaction with groundwater preferentially leaches ^{234}U from these surface-enriched zones, progressively lowering the ($^{234}U/^{238}U$) activity ratio in the residual solid phase toward secular equilibrium (~1), as illustrated in Fig S10. In oxidizing conditions, U is released from the mineral lattice without isotopic fractionation; however, due to the surface enrichment of ^{234}U due to recoil effect, the dissolved U exhibits slightly elevated ($^{234}U/^{238}U$) ratios relative to the solid. This effect is apparent in the northeastern part of the Arikaree aquifer, where oxidizing conditions dominate. Groundwater samples from this region show the highest U concentrations (23–48 µg/L), $\delta^{238}U$ values around 0.33‰, and ($^{234}U/^{238}U$) activity ratios between 1.53 and 1.8 values that reflect the imprint of ^{234}U-enriched grain boundaries in the U rich source rock. In contrast, the northwestern and southwestern portions of the aquifer are more reducing, which limits the oxidative dissolution of U(IV). Yet, groundwater in these regions also shows ($^{234}U/^{238}U$) activity ratios in the lower range (1.53–1.8). This pattern suggests that even under reducing conditions, minor desorption of ^{234}U—generated by alpha decay of ^{238}U—can occur at grain boundaries. Such desorption may elevate the ($^{234}U/^{238}U$) ratio slightly, even in the absence of significant mineral dissolution. These observations highlight that, regardless of redox conditions, the U activity ratio remains a valuable indicator of proximity to uranium source material.

In comparison, samples with ($^{234}U/^{238}U$) ranging from 1.83 to 2.5 reflect U that has been transported over longer distances along groundwater flow paths. As groundwater migrates, ^{234}U accumulates due to ongoing decay of ^{238}U and continued leaching from mineral surfaces. This characteristic U isotopic signature helps distinguish groundwater in contact with sandstone-hosted U deposit from groundwater where U has been remobilized and transported away from its source.

By integrating U concentrations, $\delta^{238}U$ values, ($^{234}U/^{238}U$) activity ratios, and redox-sensitive elements (Fe, Mn, Se, and V), we identify two distinct hydrogeochemical regimes controlling U mobility in this region. In the northeastern downgradient section marked as Zone A (Fig 2), oxidative dissolution actively mobilizes U, leading to the highest U concentrations (23–48 µg/L). The higher $\delta^{238}U$ values

(~0.3‰), low Fe and Mn concentrations, and elevated Se and V concentrations confirm persistent oxidizing conditions, keeping U in its soluble form. Groundwater in this region maintains a relatively lower ($^{234}U/^{238}U$) activity ratio (1.53–1.80), consistent with oxidative dissolution of U minerals. In contrast, in the western section marked as Zone B, lower U concentrations along with lower $\delta^{238}U$ values (-1.06‰ to -0.14‰) and elevated Fe (24–752 µg/L) and Mn (228–997 µg/L) concentrations indicate active U(VI) reduction. Zone B serves as a natural attenuation zone for U, where naturally occurring reducing conditions promotes U removal from groundwater. The depletion of Se and V further supports this interpretation, as both elements, like U, forms insoluble species under reducing conditions. The higher U activity ratios (≥1.83) in this region suggest longer transport of U from its source. This spatial redox pattern dictates whether U persists in groundwater (zone A) or is removed (zone B) and shapes the long-term fate and transport of U in the aquifer.

Presence of four predominant geochemical environments: The cluster analysis identified four major clusters, and a fifth grouping of outlier with three samples, which were not considered further in any statistical or geochemical interpretation (Fig. 4). Samples from each of the four significant groupings are presented in box and whisker diagrams (Fig. S11-14), which highlight the differences in groundwater geochemistry within the dataset.

Distinct geochemical patterns emerge across clusters based on $\delta^{238}U$, ($^{234}U/^{238}U$), and U concentration (Fig. S11). Cluster 1 has the highest median U concentration (18 µg/L), with 25% of samples exceeding the USEPA MCL of 30 µg/L. Cluster 4 also shows elevated U levels (median: 19 µg/L), with 10% of samples in this cluster exceeding the USEPA MCL of 30 µg/L. In contrast, Clusters 2 and 3 have significantly lower median U concentrations—8.3 and 6.2 µg/L, respectively—and are not significantly different from each other ($p = 0.250$). Variations in $\delta^{238}U$ and ($^{234}U/^{238}U$) across clusters are minor. Cluster 1 has a median $\delta^{238}U$ of -0.16‰, with 28% of samples showing more positive values, which indicate more oxidizing conditions. Cluster 2 exhibits the lowest $\delta^{238}U$ values (median: -0.23‰), which indicate relatively more reducing conditions. While ($^{234}U/^{238}U$) ratios do not differ significantly across clusters ($p = 0.333$), 70% of Cluster 3 samples have values >1.8. This enrichment of ^{234}U indicate U transport away from its

source, driven by ongoing ^{238}U decay and preferential ^{234}U leaching from aquifer materials during transport. In contrast, 40% of Cluster 4 samples fall within the 1.53–1.80 range, consistent with proximity to U deposits.

Differences in Mn, Fe, NO_3^-, SO_4^{2-}, Se, and V concentrations across the four clusters underscore the geochemical contrasts and further support the redox interpretations based on $\delta^{238}U$ data (SI, Fig. S12-13). Dissolved NO_3^- concentrations do not show statistically significant differences across clusters, the median values follow the same pattern as $\delta^{238}U$, and the highest NO_3^- concentrations (median: 4 mg/L) observed in Cluster 1. Cluster 2 has the highest Mn (median: 383 µg/L) and Fe (median: 27 µg/L) concentrations. These values indicate active Mn (IV) and Fe (III) reduction, the latter of which promote U(VI) reduction. This is consistent with the observed lower $\delta^{238}U$ values in this cluster. In contrast, all other clusters except cluster 2 display median Fe and Mn concentrations of less than 2 µg/L. In addition, Se and V concentrations are significantly lower in Clusters 2–4 than in Cluster 1. Elevated Se and V in Cluster 1 point to more oxidizing conditions, while their depletion in Cluster 2 supports the presence of strongly reducing conditions. The consistent trends in these redox-sensitive elements reinforce the redox classification based on U isotope data and highlight the spatial geochemical controls on U mobility in the study area.

PCA further supports the presence of four geochemical environments. Principal Component Analysis (PCA) confirms the presence of four distinct geochemical environments in the study area. The first two principal components (PC1 and PC2) account for 28% of the total variance (SI, Fig. S15), and provide key insights into the dominant geochemical processes. PC1 vs. PC2 plots clearly delineate geochemical differences across the study area (Fig. 5). The direction and magnitude of loadings indicate how strongly each variable contributes to a principal component; longer vectors correspond to greater influence. PC1 is dominated by Fe, Mn, Eh, and ($^{234}U/^{238}U$) and primarily reflects reducing condition. The strong loading of Mn and Fe suggests an association with Mn (IV) and Fe (III) reducing environments, while variations in ($^{234}U/^{238}U$) likely reflect groundwater U transport time. This suggests that ($^{234}U/^{238}U$) is more influenced by transport rather than U reduction. PC2 is driven by Se, V, As, and U, which are

indicative of oxidizing conditions. Cluster distribution in PCA space reflects these geochemical trends: Cluster 1 (positive PC2, negative PC1) corresponds to a strongly oxidizing environment with minimal reduction. Cluster 2 (negative PC2, positive PC1) represents Mn (IV) and Fe (III) reducing conditions, latter of which drives U(VI) reduction. Clusters 3 and 4 overlap slightly and represent a transitional phase between oxidized and reduced U conditions. Cluster 4 is characterized by high U loadings and low ($^{234}U/^{238}U$), which indicate proximity to a U source and strongly oxidizing conditions.

The spatial distribution of clusters across the study area reveals distinct redox zones and U mobility patterns, which provide critical insights into aquifer geochemistry (Fig. 1). Cluster 1, associated with oxidizing conditions, occurs in the northeastern region of the study area. In this region, oxidative dissolution mobilizes U, which leads to elevated concentrations and higher $\delta^{238}U$ values (−0.08‰ to 0.30‰). Cluster 2 represents reducing conditions and is concentrated in the southwestern part of the study area, where U undergoes removal from groundwater through reduction and precipitation. This process inhibits U transport. Cluster 3 shows no clear spatial pattern and appears dispersed across the study area, which indicates the presence of transitional zones with inconsistent redox conditions. Cluster 4, characterized by high U concentrations and low ($^{234}U/^{238}U$) activity ratios, is strongly aligned with mineralized zones in the downgradient portion of the aquifer. These spatial trends show that U transport in the aquifer is controlled by oxidation-driven mobility in the northeast, reduction-driven retention in the southwest, and localized release from mineralized zones in the central and southern part of the aquifer.

Environmental Implications: In a large-scale aquifer system like the one beneath our study area, where sampling is limited and sampling locations are widely spaced, U isotopes serve as a powerful tool for identifying zones of groundwater U release and removal. The spatial patterns of $\delta^{238}U$ clearly delineate zones of U reduction, a process further supported by Fe and other redox-sensitive elements. Unlike U concentrations, which may remain stable if reaction kinetics are slow or a steady state is reached, U isotopic shifts in groundwater provide as a more sensitive and direct tracer of reductive removal. It is important to note that the presence of Mn (IV)- and Fe (III)-reducing conditions does not definitively indicate U(VI) reduction. Under these conditions, U(VI) reduction may be kinetically limited, meaning the

445 reaction rate is too slow to cause an immediate decline in U concentrations. Thus, even when the reduction
446 is slow and only partial, shifts in $\delta^{238}U$ and ($^{234}U/^{238}U$) ratios provide clear evidence of ongoing U(VI)
447 reduction. Therefore, by integrating $\delta^{238}U$, ($^{234}U/^{238}U$), and statistical and spatial analyses, our approach
448 delivers a comprehensive framework for understanding U mobility and redox evolution in complex aquifer
449 systems. Beyond its diagnostic role, our U isotope approach provides critical insights for remediation by
450 pinpointing areas where U is actively reduced and immobilized. Understanding redox conditions governing
451 U behavior is key to effective in-situ U(VI) remediation, as aggressive reduction can mobilize As from Fe-
452 oxides under strongly reducing conditions and pose a risk to groundwater quality.

453 While U isotopic measurements provide a valuable spatial snapshot, they do not capture temporal
454 variations in U concentrations or corresponding isotopic shifts. A more comprehensive understanding of
455 redox dynamics and long-term U mobility requires time-series data on U(VI) concentrations and $\delta^{238}U$ from
456 private wells across this region. However, the irregular distribution of private wells, dictated by population
457 density, distance between households, water access and affordability, limits the ability to monitor U
458 transport at a fine spatial resolution. Additionally, the presence of mineralized zones at localized scales (tens
459 to hundreds of meters) complicates the interpretation of U migration pathways. Given that well locations
460 are not evenly spaced and do not always align with geochemically significant zones, sampling gaps restrict
461 the resolution of spatial trends in U cycling. Dedicated monitoring wells would address this limitation, but
462 such efforts are often logistically and financially impractical. Future studies should prioritize targeted
463 investigations in key locations, particularly in the northeastern part (zone 1) of the Arikaree aquifer, where
464 U concentrations are expected to increase due to continued oxidative dissolution of U-bearing minerals.
465 Despite these limitations, the integration of U isotopic tracers, hydrochemical data, and spatial analysis
466 remains a powerful approach for assessing U mobility in data-scarce regions. We will work with MBIRI to
467 share findings directly with tribal committees and through community meetings. Risk maps and key
468 messages will be translated into native languages with support from local artists and translators to ensure
469 cultural accessibility. These results will inform mitigation strategies in high-risk areas and support
470 community-driven solutions, such as well testing, water treatment, and safe water access.

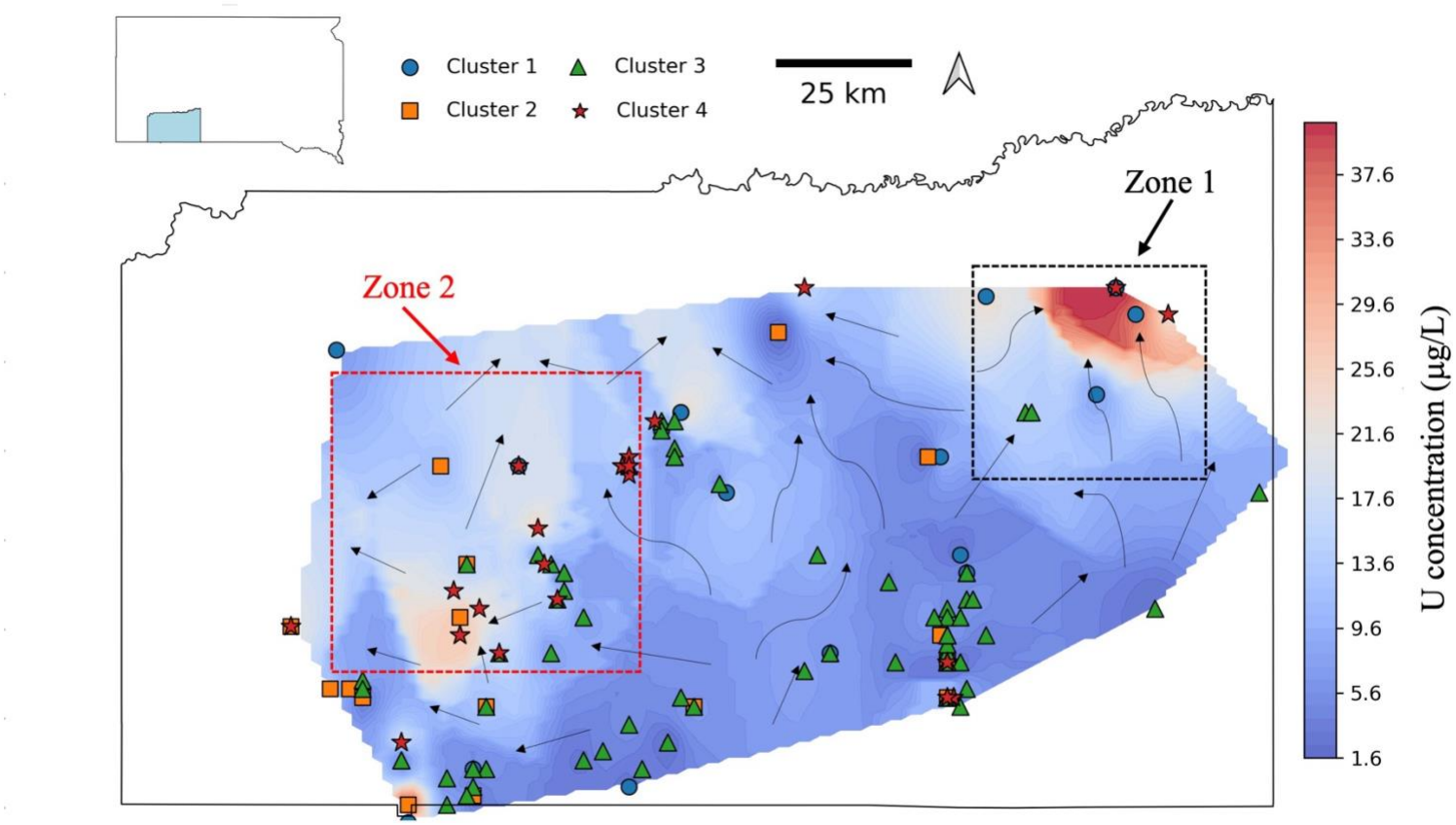

Figure 1: Spatial distribution of uranium (U) concentrations (µg/L) in groundwater samples (n=140) across the study region. The heatmap is generated using kriging, with warm colors (red) indicating higher U concentrations and cool colors (blue) representing lower concentrations. The different symbols denote K-means cluster assigned sampling locations. The inset map shows the location of Pine Ridge Reservation in southwest South Dakota. A scale bar and north arrow are included for spatial reference.

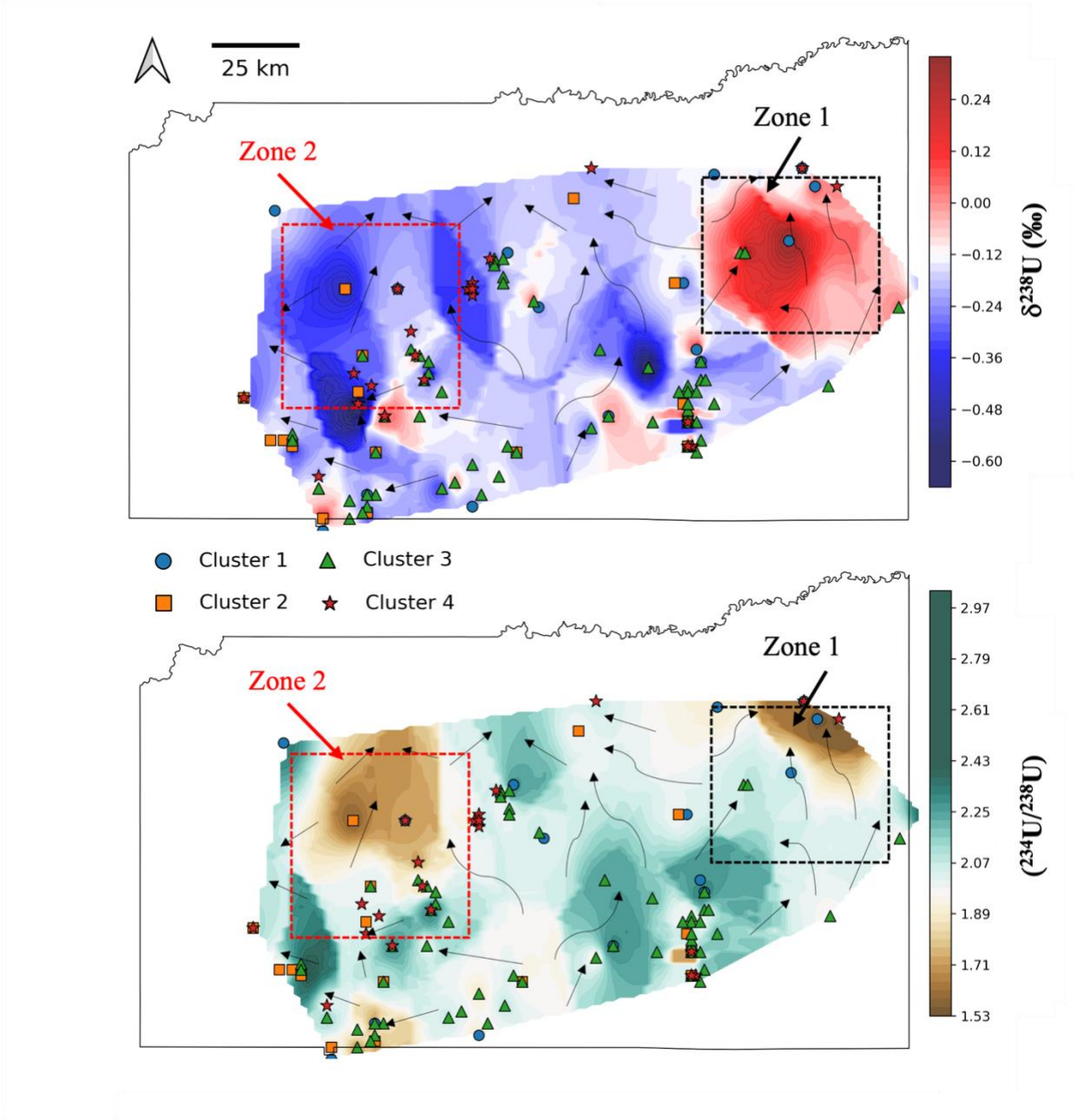

Figure 2: Spatial distribution of $\delta^{238}U$ and ($^{234}U/^{238}U$) in groundwater samples (n=140) across the study region. **(Top)**: Groundwater $\delta^{238}U$ isoscapes showing warm colors (red) indicate more positive values and cool colors (blue) represent more negative values. **(Bottom)**: Spatial variation of groundwater U activity ratio ($^{234}U/^{238}U$), with darker shades indicating lower ratios close to 1. Different symbols represent groundwater sampling locations according to their cluster assignments. Both maps utilize kriging interpolation to illustrate regional trends, with a scale bar and north arrow for spatial reference

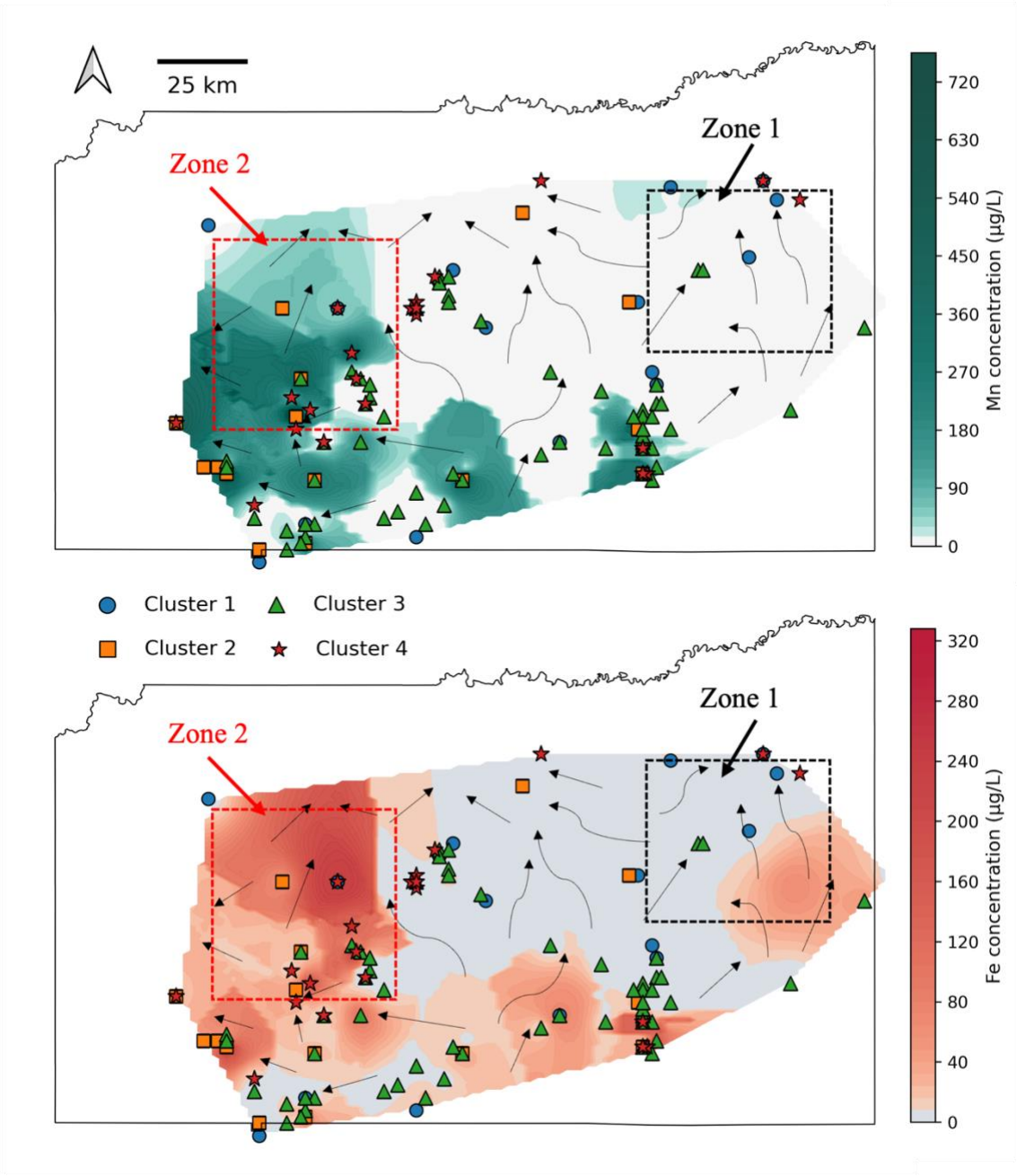

Figure 3: Spatial distribution of manganese (Mn) and iron (Fe) levels with groundwater flow direction. The unit of Mn and Fe concentration is µg/L. Different symbols represent groundwater sampling locations (n=141) based on their cluster assignments. Both maps utilize IDW interpolation to illustrate regional trends, with a scale bar and north arrow for spatial reference. The black arrows indicate groundwater flow path, traced from published studies.[50]

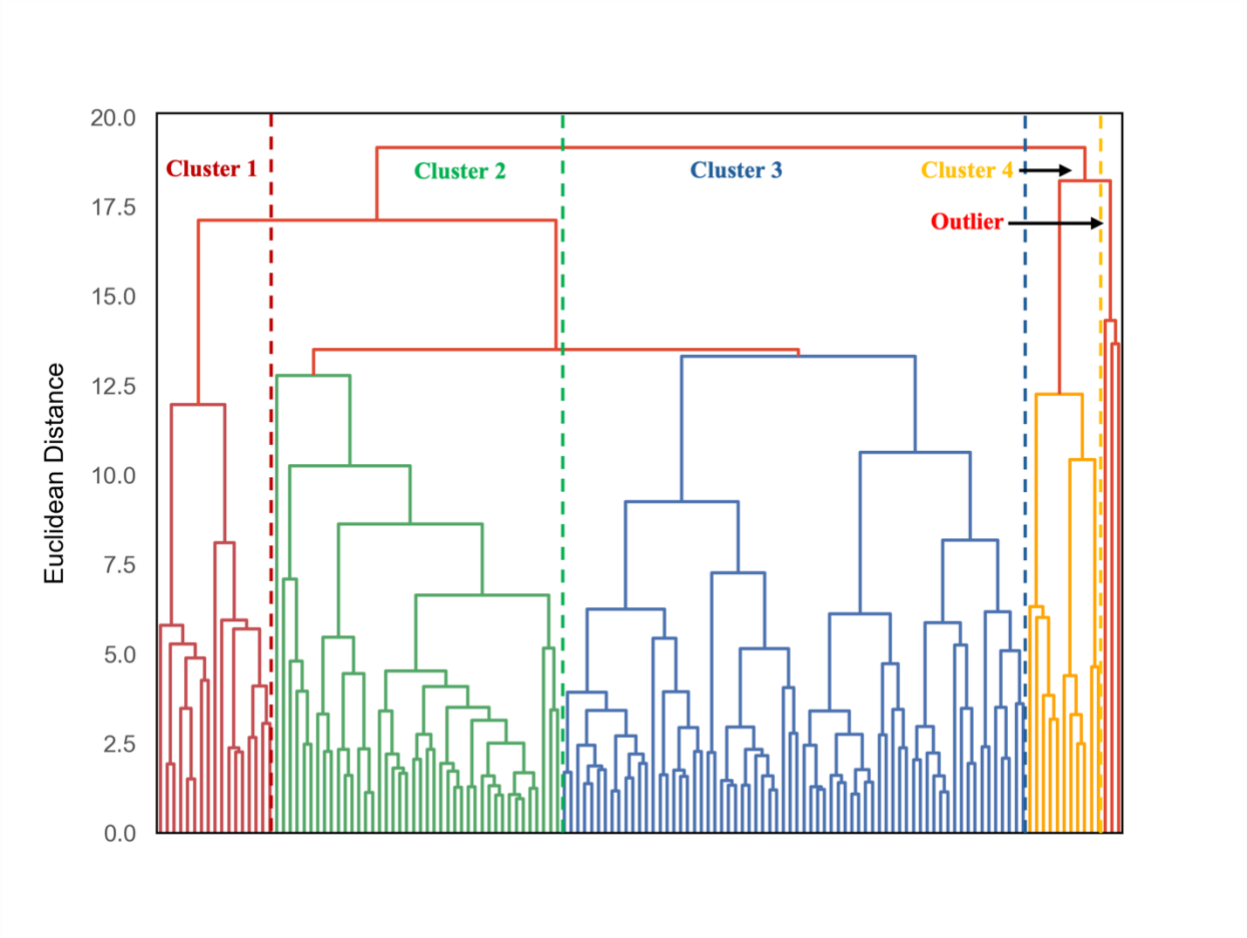

Figure 4: Dendrogram of Q-mode analysis of the study area water chemistry. There are four distinct clusters that can be seen in this analysis. Each of the four significant groupings was assigned a color, from left to right: red, green, blue and yellow.

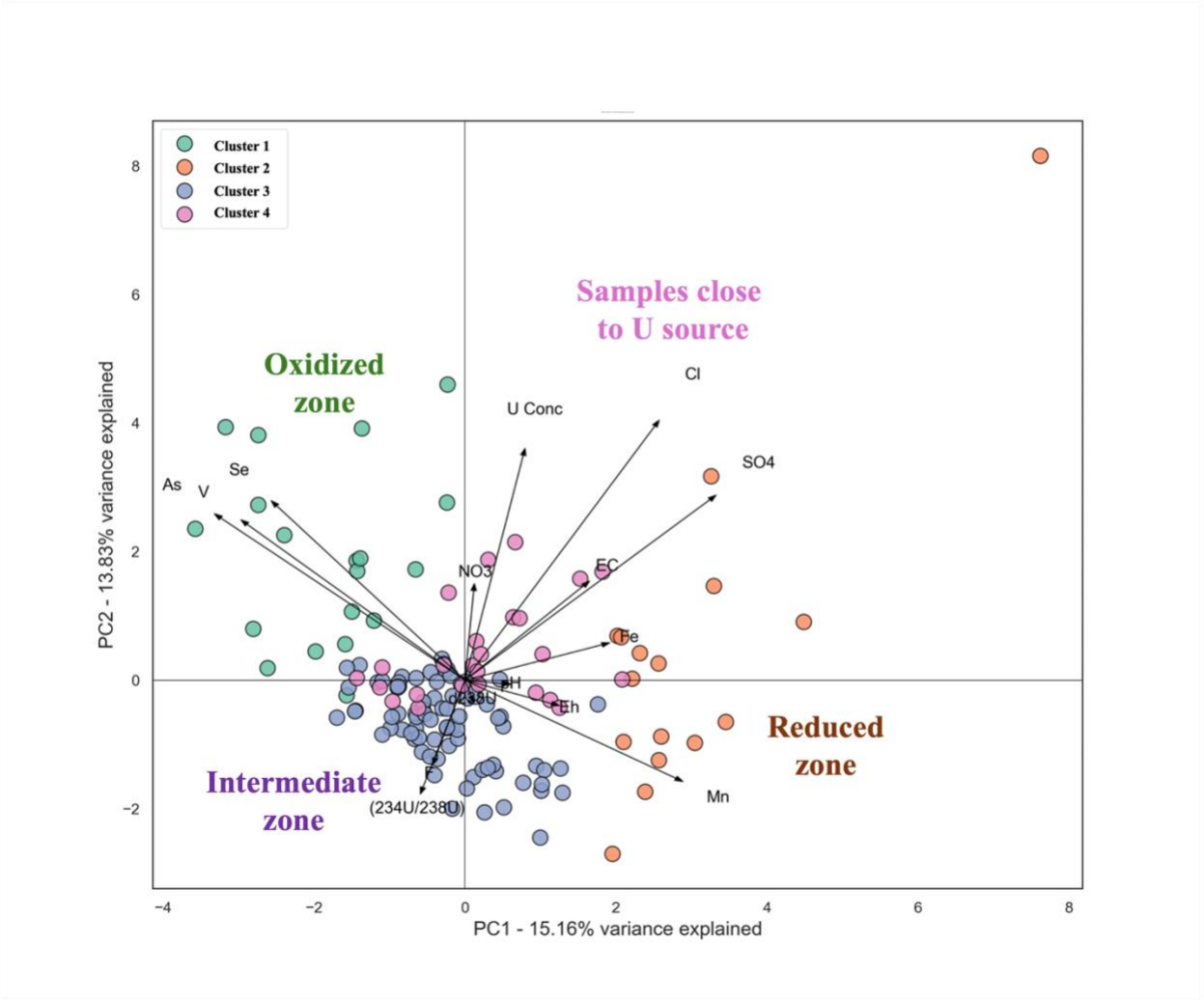

Figure 5: Biplots of the two principal components (PC1 and PC2), showing separation of geochemical regions and relative importance of geochemical parameters on delineating geochemical regions (the magnitude of the vector indicates its relative importance on each of the principal components). PCA-transformed data for each sample are plotted as circles and vectors for each of the geochemical parameters are plotted as black lines with arrowhead.

ASSOCIATED CONTENT

Supporting Information. Details of the site background, analytical procedures, information related to groundwater samples (GPS coordinates, field parameters, NO_3^-, SO_4^{2-}), groundwater trace element concentrations, $\delta^{238}U$ and ($^{234}U/^{238}U$) values.

AUTHOR INFORMATION

Corresponding Author

*Arijeet Mitra (am6368@cumc.columbia.edu) , Department of Environmental Health Sciences, Mailman School of Public Health, Columbia University, New York, NY 10032

Author Contributions

A.B. designed and supervised the study. R.H., T.Z., R.O., A.M., S.A., did the field work. J.R., S.C., M.S., conducted the trace metal and anion concentration measurements. A.M. conducted isotopic measurements. A.M., and S.A. conducted the statistical analysis. A.B. and K.S. contributed to U isotope analysis. A.M., A.B., and K.S. wrote the paper with input from all authors.

ACKNOWLEDGMENT

The work was supported by the NIEHS funded Columbia University Northern Plains Superfund program (P42ES033719). The NICER Lab is supported by funding to A.N.H. from Columbia University.

References

(1) Jones, D. S. The Persistence of American Indian Health Disparities. *Am J Public Health* **2006**, *96* (12), 2122–2134. https://doi.org/10.2105/AJPH.2004.054262.

(2) Mitchell, F. M. Water (in)Security and American Indian Health: Social and Environmental Justice Implications for Policy, Practice, and Research. *Public Health* **2019**, *176*, 98–105. https://doi.org/https://doi.org/10.1016/j.puhe.2018.10.010.

(3) Indian Health Service (IHS). *Safe Water and Waste Disposal Facilities*; Rockville MD, 2013.

(4) Mitchell, F. M. Water (in)Security and American Indian Health: Social and Environmental Justice Implications for Policy, Practice, and Research. *Public Health* **2019**, *176*, 98–105. https://doi.org/https://doi.org/10.1016/j.puhe.2018.10.010.

(5) Ravalli, F.; Yu, Y.; Bostick, B. C.; Chillrud, S. N.; Schilling, K.; Basu, A.; Navas-Acien, A.; Nigra, A. E. Sociodemographic Inequalities in Uranium and Other Metals in Community Water Systems across the USA, 2006–11: A Cross-Sectional Study. *Lancet Planet Health* **2022**, *6* (4), e320–e330. https://doi.org/10.1016/S2542-5196(22)00043-2.

(6) Jones, L.; Credo, J.; Parnell, R.; Ingram, J. C. Dissolved Uranium and Arsenic in Unregulated Groundwater Sources – Western Navajo Nation. *J Contemp Water Res Educ* **2020**, *169* (1), 27–43. https://doi.org/https://doi.org/10.1111/j.1936-704X.2020.03330.x.

(7) Lewis, J.; Hoover, J.; MacKenzie, D. Mining and Environmental Health Disparities in Native American Communities. *Current environmental health reports*. Springer June 1, 2017, pp 130–141. https://doi.org/10.1007/s40572-017-0140-5.

(8) Hoover, J.; Gonzales, M.; Shuey, C.; Barney, Y.; Lewis, J. Elevated Arsenic and Uranium Concentrations in Unregulated Water Sources on the Navajo Nation, USA. *Expo Health* **2017**, *9* (2), 113–124. https://doi.org/10.1007/s12403-016-0226-6.

(9) Eggers, M. J.; Moore-Nall, A. L.; Doyle, J. T.; Lefthand, M. J.; Young, S. L.; Bends, A. L.; Committee, C. E. H. S.; Camper, A. K. Potential Health Risks from Uranium in Home Well Water: An Investigation by the Apsaalooke (Crow) Tribal Research Group. *Geosciences (Basel)* **2015**, *5* (1), 67–94. https://doi.org/10.3390/geosciences5010067.

(10) Swift Bird, K.; Navarre-Sitchler, A.; Singha, K. Hydrogeological Controls of Arsenic and Uranium Dissolution into Groundwater of the Pine Ridge Reservation, South Dakota. *Applied Geochemistry* **2020**, *114*, 104522. https://doi.org/https://doi.org/10.1016/j.apgeochem.2020.104522.

(11) Sobel, M.; Sanchez, T. R.; Zacher, T.; Mailloux, B.; Powers, M.; Yracheta, J.; Harvey, D.; Best, L. G.; Bear, A. B.; Hasan, K.; Thomas, E.; Morgan, C.; Aurand, D.; Ristau, S.; Olmedo, P.; Chen, R.; Rule, A.; O'Leary, M.; Navas-Acien, A.; George, C. M.; Bostick, B. Spatial Relationship between Well Water Arsenic and Uranium in Northern Plains Native Lands. *Environmental Pollution* **2021**, *287*. https://doi.org/10.1016/j.envpol.2021.117655.

(12) Rogers, D.; Petereit, D. G. Cancer Disparities Research Partnership in Lakota Country: Clinical Trials, Patient Services, and Community Education for the Oglala, Rosebud, and Cheyenne River Sioux Tribes. *Am J Public Health* **2005**, *95* (12), 2129–2132. https://doi.org/10.2105/AJPH.2004.053645.

(13) Ana, N.-A.; G, U. J.; V, H. B.; Walter, G.; A, F. K.; M, C. C.; K, S. E.; Eliseo, G. Urine Arsenic Concentrations and Species Excretion Patterns in American Indian Communities Over a 10-Year Period: The Strong Heart Study. *Environ Health Perspect* **2009**, *117* (9), 1428–1433. https://doi.org/10.1289/ehp.0800509.

(14) Pang, Y.; Peng, R. D.; Jones, M. R.; Francesconi, K. A.; Goessler, W.; Howard, B. V; Umans, J. G.; Best, L. G.; Guallar, E.; Post, W. S.; Kaufman, J. D.; Vaidya, D.; Navas-Acien, A. Metal Mixtures in Urban and Rural Populations in the US: The Multi-Ethnic Study of Atherosclerosis and the Strong Heart Study. *Environ Res* **2016**, *147*, 356–364. https://doi.org/https://doi.org/10.1016/j.envres.2016.02.032.

(15) Larson, L. N.; Kipp, G. G.; Mott, H. V; Stone, J. J. Sediment Pore-Water Interactions Associated with Arsenic and Uranium Transport from the North Cave Hills Mining Region, South Dakota, USA. *Applied Geochemistry* **2012**, *27* (4), 879–891. https://doi.org/https://doi.org/10.1016/j.apgeochem.2012.01.008.

(16) Sharma, R. K.; Putirka, K. D.; Stone, J. J. Stream Sediment Geochemistry of the Upper Cheyenne River Watershed within the Abandoned Uranium Mining Region of the Southern Black Hills, South Dakota, USA. *Environ Earth Sci* **2016**, *75* (9), 823. https://doi.org/10.1007/s12665-016-5522-8.

(17) Rahn, P. H.; Davis, A. D.; Webb, C. J.; Nichols, A. D. Water Quality Impacts from Mining in the Black Hills, South Dakota, USA. *Environmental Geology* **1996**, *27* (1), 38–53. https://doi.org/10.1007/BF00770601.

(18) Robinson, C. S.; Gott, G. B. *Uranium Deposits of the Black Hills, South Dakota and Wyoming*; 1958. https://doi.org/10.3133/tei723.

(19) Dahlkamp, F. J. Northern Great Plains. In *Uranium Deposits of the World: USA and Latin America*; Dahlkamp, F. J., Ed.; Springer Berlin Heidelberg: Berlin, Heidelberg, 2010; pp 219–232. https://doi.org/10.1007/978-3-540-78943-7_5.

(20) Lovley, D. R.; Phillips, E. J. P.; Gorby, Y. A.; Landa, E. R. Microbial Reduction of Uranium. *Nature* **1991**, *350* (6317), 413–416. https://doi.org/10.1038/350413a0.

(21) Sani, R. K.; Peyton, B. M.; Amonette, J. E.; Geesey, G. G. Reduction of Uranium(VI) under Sulfate-Reducing Conditions in the Presence of Fe(III)-(Hydr)Oxides1 1Associate Editor: C. M. Eggleston. *Geochim Cosmochim Acta* **2004**, *68* (12), 2639–2648. https://doi.org/https://doi.org/10.1016/j.gca.2004.01.005.

(22) R, S. J.; A, F. L.; D, H. B. Modeling Reduction of Uranium U(VI) under Variable Sulfate Concentrations by Sulfate-Reducing Bacteria. *Appl Environ Microbiol* **2000**, *66* (9), 3711–3721. https://doi.org/10.1128/AEM.66.9.3711-3721.2000.

(23) Komlos, J.; Peacock, A.; Kukkadapu, R. K.; Jaffé, P. R. Long-Term Dynamics of Uranium Reduction/Reoxidation under Low Sulfate Conditions. *Geochim Cosmochim Acta* **2008**, *72* (15), 3603–3615. https://doi.org/https://doi.org/10.1016/j.gca.2008.05.040.

(24) Moon, H. S.; McGuinness, L.; Kukkadapu, R. K.; Peacock, A. D.; Komlos, J.; Kerkhof, L. J.; Long, P. E.; Jaffé, P. R. Microbial Reduction of Uranium under Iron- and Sulfate-

Reducing Conditions: Effect of Amended Goethite on Microbial Community Composition and Dynamics. *Water Res* **2010**, *44* (14), 4015–4028. https://doi.org/https://doi.org/10.1016/j.watres.2010.05.003.

(25) Sani, R. K.; Peyton, B. M.; Dohnalkova, A.; Amonette, J. E. Reoxidation of Reduced Uranium with Iron(III) (Hydr)Oxides under Sulfate-Reducing Conditions. *Environ Sci Technol* **2005**, *39* (7), 2059–2066. https://doi.org/10.1021/es0494297.

(26) Lovley, D. R.; Roden, E. E.; Phillips, E. J. P.; Woodward, J. C. Enzymatic Iron and Uranium Reduction by Sulfate-Reducing Bacteria. *Mar Geol* **1993**, *113* (1), 41–53. https://doi.org/https://doi.org/10.1016/0025-3227(93)90148-O.

(27) Westrop, J. P.; Yadav, P.; Nolan, P. J.; Campbell, K. M.; Singh, R.; Bone, S. E.; Chan, A. H.; Kohtz, A. J.; Pan, D.; Healy, O.; Bargar, J. R.; Snow, D. D.; Weber, K. A. Nitrate-Stimulated Release of Naturally Occurring Sedimentary Uranium. *Environ Sci Technol* **2023**, *57* (10), 4354–4366. https://doi.org/10.1021/acs.est.2c07683.

(28) Nolan, J.; Weber, K. A. Natural Uranium Contamination in Major U.S. Aquifers Linked to Nitrate. *Environ Sci Technol Lett* **2015**, *2* (8), 215–220. https://doi.org/10.1021/acs.estlett.5b00174.

(29) Brown, S. T.; Basu, A.; Ding, X.; Christensen, J. N.; DePaolo, D. J. Uranium Isotope Fractionation by Abiotic Reductive Precipitation. *Proc Natl Acad Sci U S A* **2018**, *115* (35), 8688–8693. https://doi.org/10.1073/pnas.1805234115.

(30) Basu, A.; Sanford, R. A.; Johnson, T. M.; Lundstrom, C. C.; Löffler, F. E. Uranium Isotopic Fractionation Factors during U(VI) Reduction by Bacterial Isolates. *Geochim Cosmochim Acta* **2014**, *136*, 100–113. https://doi.org/https://doi.org/10.1016/j.gca.2014.02.041.

(31) Brown, S. T.; Basu, A.; Christensen, J. N.; Reimus, P.; Heikoop, J.; Simmons, A.; Woldegabriel, G.; Maher, K.; Weaver, K.; Clay, J.; DePaolo, D. J. Isotopic Evidence for Reductive Immobilization of Uranium Across a Roll-Front Mineral Deposit. *Environ Sci Technol* **2016**, *50* (12), 6189–6198. https://doi.org/10.1021/acs.est.6b00626.

(32) Basu, A.; Wanner, C.; Johnson, T. M.; Lundstrom, C. C.; Sanford, R. A. 4; Sonnenthal, E. L.; Boyanov, M. I.; Kemner, K. M. *Microbial U Isotope Fractionation Depends on U(VI) 2 Reduction Rate*.

(33) Abe, M.; Suzuki, T.; Fujii, Y.; Hada, M.; Hirao, K. An Ab Initio Molecular Orbital Study of the Nuclear Volume Effects in Uranium Isotope Fractionations. *J Chem Phys* **2008**, *129* (16), 164309. https://doi.org/10.1063/1.2992616.

(34) Bigeleisen, J. Nuclear Size and Shape Effects in Chemical Reactions. Isotope Chemistry of the Heavy Elements. *J Am Chem Soc* **1996**, *118* (15), 3676–3680. https://doi.org/10.1021/ja954076k.

(35) Schauble, E. A. Role of Nuclear Volume in Driving Equilibrium Stable Isotope Fractionation of Mercury, Thallium, and Other Very Heavy Elements. *Geochim Cosmochim Acta* **2007**, *71* (9), 2170–2189. https://doi.org/https://doi.org/10.1016/j.gca.2007.02.004.

(36) Basu, A.; Sanford, R. A.; Johnson, T. M.; Lundstrom, C. C.; Löffler, F. E. Uranium Isotopic Fractionation Factors during U(VI) Reduction by Bacterial Isolates. *Geochim Cosmochim Acta* **2014**, *136*, 100–113. https://doi.org/https://doi.org/10.1016/j.gca.2014.02.041.

(37) Basu, A.; Wanner, C.; Johnson, T. M.; Lundstrom, C. C.; Sanford, R. A.; Sonnenthal, E. L.; Boyanov, M. I.; Kemner, K. M. Microbial U Isotope Fractionation Depends on the U(VI) Reduction Rate. *Environ Sci Technol* **2020**, *54* (4), 2295–2303. https://doi.org/10.1021/acs.est.9b05935.
(38) Jemison, N. E.; Johnson, T. M.; Shiel, A. E.; Lundstrom, C. C. Uranium Isotopic Fractionation Induced by U(VI) Adsorption onto Common Aquifer Minerals. *Environ Sci Technol* **2016**, *50* (22), 12232–12240. https://doi.org/10.1021/acs.est.6b03488.
(39) Brennecka, G. A.; Wasylenki, L. E.; Bargar, J. R.; Weyer, S.; Anbar, A. D. Uranium Isotope Fractionation during Adsorption to Mn-Oxyhydroxides. *Environ Sci Technol* **2011**, *45* (4), 1370–1375. https://doi.org/10.1021/es103061v.
(40) Kigoshi, K. Alpha-Recoil Thorium-234: Dissolution into Water and the Uranium-234/Uranium-238 Disequilibrium in Nature. *Science (1979)* **1971**, *173* (3991), 47–48. https://doi.org/10.1126/science.173.3991.47.
(41) Maher, K.; DePaolo, D. J.; Christensen, J. N. U–Sr Isotopic Speedometer: Fluid Flow and Chemical Weathering Rates in Aquifers. *Geochim Cosmochim Acta* **2006**, *70* (17), 4417–4435. https://doi.org/https://doi.org/10.1016/j.gca.2006.06.1559.
(42) DePaolo, D. J.; Lee, V. E.; Christensen, J. N.; Maher, K. Uranium Comminution Ages: Sediment Transport and Deposition Time Scales. *Comptes Rendus Geoscience* **2012**, *344* (11), 678–687. https://doi.org/https://doi.org/10.1016/j.crte.2012.10.014.
(43) Lee, V. E.; DePaolo, D. J.; Christensen, J. N. Uranium-Series Comminution Ages of Continental Sediments: Case Study of a Pleistocene Alluvial Fan. *Earth Planet Sci Lett* **2010**, *296* (3), 244–254. https://doi.org/https://doi.org/10.1016/j.epsl.2010.05.005.
(44) DePaolo, D. J.; Maher, K.; Christensen, J. N.; McManus, J. Sediment Transport Time Measured with U-Series Isotopes: Results from ODP North Atlantic Drift Site 984. *Earth Planet Sci Lett* **2006**, *248* (1), 394–410. https://doi.org/https://doi.org/10.1016/j.epsl.2006.06.004.
(45) Basu, A.; Brown, S. T.; Christensen, J. N.; DePaolo, D. J.; Reimus, P. W.; Heikoop, J. M.; Woldegabriel, G.; Simmons, A. M.; House, B. M.; Hartmann, M.; Maher, K. Isotopic and Geochemical Tracers for U(VI) Reduction and U Mobility at an in Situ Recovery U Mine. *Environ Sci Technol* **2015**, *49* (10), 5939–5947. https://doi.org/10.1021/acs.est.5b00701.
(46) Spaur, M.; Glabonjat, R. A.; Schilling, K.; Lombard, M. A.; Galvez-Fernandez, M.; Lieberman-Cribbin, W.; Hayek, C.; Ilievski, V.; Balac, O.; Izuchukwu, C.; Patterson, K.; Basu, A.; Bostick, B. C.; Chen, Q.; Sanchez, T.; Navas-Acien, A.; Nigra, A. E. Contribution of Arsenic and Uranium in Private Wells and Community Water Systems to Urinary Biomarkers in US Adults: The Strong Heart Study and the Multi-Ethnic Study of Atherosclerosis. *J Expo Sci Environ Epidemiol* **2024**, *34* (1), 77–89. https://doi.org/10.1038/s41370-023-00586-2.
(47) Thomas, E. D.; Gittelsohn, J.; Yracheta, J.; Powers, M.; O'Leary, M.; Harvey, D. E.; Red Cloud, R.; Best, L. G.; Black Bear, A.; Navas-Acien, A.; George, C. M. The Strong Heart Water Study: Informing and Designing a Multi-Level Intervention to Reduce Arsenic Exposure among Private Well Users in Great Plains Indian Nations. *Science of The*

Total Environment **2019**, *650*, 3120–3133. https://doi.org/https://doi.org/10.1016/j.scitotenv.2018.09.204.

(48) Zacher, T.; Endres, K.; Richards, F.; Robe, L. B.; Powers, M.; Yracheta, J.; Harvey, D.; Best, L. G.; Red Cloud, R.; Black Bear, A.; Ristau, S.; Aurand, D.; Skinner, L.; Cuny, C.; Gross, M.; Thomas, E.; Rule, A.; Schwab, K. J.; O'Leary, M.; Moulton, L. H.; Navas-Acien, A.; George, C. M. Evaluation of a Water Arsenic Filter in a Participatory Intervention to Reduce Arsenic Exposure in American Indian Communities: The Strong Heart Water Study. *Science of The Total Environment* **2023**, *862*, 160217. https://doi.org/https://doi.org/10.1016/j.scitotenv.2022.160217.

(49) Lieberman-Cribbin, W.; Domingo-Relloso, A.; Glabonjat, R. A.; Schilling, K.; Cole, S. A.; O'Leary, M.; Best, L. G.; Zhang, Y.; Fretts, A. M.; Umans, J. G.; Goessler, W.; Navas-Acien, A.; Tellez-Plaza, M.; Kupsco, A. An Epigenome-Wide Study of Selenium Status and DNA Methylation in the Strong Heart Study. *Environ Int* **2024**, *191*, 108955. https://doi.org/https://doi.org/10.1016/j.envint.2024.108955.

(50) Patterson, K. P.; Nigra, A. E.; Olmedo, P.; Grau-Perez, M.; O'Leary, R.; O'Leary, M.; Fretts, A. M.; Umans, J. G.; Best, L. G.; Goessler, W.; Cole, S. A.; Navas-Acien, A. Geographic and Dietary Differences of Urinary Uranium Levels in the Strong Heart Family Study. *J Expo Sci Environ Epidemiol* **2025**, *35* (3), 393–402. https://doi.org/10.1038/s41370-024-00695-6.

(51) Williams, S. C.; Navas-Acien, A.; Goessler, W.; Verney, S. P.; Erdei, E.; Buchwald, D.; Suchy-Dicey, A.; Best, L. G. Urinary Selenium, Cranial MRI, and Cognitive Function in American Indians: The Strong Heart Study. *Environ Res* **2025**, *269*, 120913. https://doi.org/https://doi.org/10.1016/j.envres.2025.120913.

(52) Marie, G. C.; Tracy, Z.; Kelly, E.; Francine, R.; Lisa, B. R.; David, H.; G, B. L.; Reno, R. C.; Annabelle, B. B.; Leslie, S.; Christa, C.; Ana, R.; J, S. K.; Joel, G.; Alexander, G. R.; Kathrin, S.; Marcia, O.; D, T. E.; Jason, U.; Jianhui, Z.; H, M. L.; Ana, N.-A. Effect of an Arsenic Mitigation Program on Arsenic Exposure in American Indian Communities: A Cluster Randomized Controlled Trial of the Community-Led Strong Heart Water Study Program. *Environ Health Perspect* **2025**, *132* (3), 037007. https://doi.org/10.1289/EHP12548.

(53) McConnell, T. H.; DiBenedetto, J. N. Geology of the Early Arikareean Sharps Formation on the Pine Ridge Indian Reservation and Surrounding Areas of South Dakota and Nebraska. *PLoS One* **2012**, *7* (10), e47759-.

(54) Sibray, S. *Potential Uranium Source Rocks of the White River Group in Western Nebraska and South Dakota**.

(55) Dickinson, K. A. *Favorable Areas for Uranium in the Oligocene White River Beds of Southwestern South Dakota, Southeastern Wyoming and Northwestern Nebraska.*; 1993.

(56) Carter, J. M.; Heakin, A. J. *Generalized Potentiometric Surface of the Arikaree Aquifer, Pine Ridge Indian Reservation and Bennett County, South Dakota*; 2007.

(57) Rahn, P. H.; Paul, H. A. Hydrogeology of a Portion of the Sand Hills and Ogallala Aquifer, South Dakota and Nebraska. *Groundwater* **1975**, *13* (5), 428–437. https://doi.org/https://doi.org/10.1111/j.1745-6584.1975.tb03610.x.

(58) Basu, A.; Brown, S. T.; Christensen, J. N.; DePaolo, D. J.; Reimus, P. W.; Heikoop, J. M.; Woldegabriel, G.; Simmons, A. M.; House, B. M.; Hartmann, M.; Maher, K. Isotopic and Geochemical Tracers for U(VI) Reduction and U Mobility at an in Situ Recovery U Mine. *Environ Sci Technol* **2015**, *49* (10), 5939–5947. https://doi.org/10.1021/acs.est.5b00701.

(59) Basu, A.; Sanford, R. A.; Johnson, T. M.; Lundstrom, C. C.; Löffler, F. E. Uranium Isotopic Fractionation Factors during U(VI) Reduction by Bacterial Isolates. *Geochim Cosmochim Acta* **2014**, *136*, 100–113. https://doi.org/10.1016/j.gca.2014.02.041.

(60) Shiel, A. E.; Laubach, P. G.; Johnson, T. M.; Lundstrom, C. C.; Long, P. E.; Williams, K. H. No Measurable Changes in 238U/235U Due to Desorption–Adsorption of U(VI) from Groundwater at the Rifle, Colorado, Integrated Field Research Challenge Site. *Environ Sci Technol* **2013**, *47* (6), 2535–2541. https://doi.org/10.1021/es303913y.

(61) Jie, C.; Hanting, Z.; Hui, Q.; Jianhua, W.; Xuedi, Z. Selecting Proper Method for Groundwater Interpolation Based on Spatial Correlation. In *2013 Fourth International Conference on Digital Manufacturing & Automation*; 2013; pp 1192–1195. https://doi.org/10.1109/ICDMA.2013.282.

(62) Xu, Q.; Jiao, Y.; Liu, C.; Liu, Z.; Ding, Y.; Zhang, H.; Tao, Y.; Zhang, Z. The Spatial Patterns and Impact Factors of Stable Oxygen and Hydrogen Isoscapes in Pond Water: A Case Study on the Water-Source Forests of the Hani Terraced Fields in Yunnan, China. *J Hydrol (Amst)* **2021**, *603*, 127097. https://doi.org/https://doi.org/10.1016/j.jhydrol.2021.127097.

(63) Scheliga, B.; Tetzlaff, D.; Nuetzmann, G.; Soulsby, C. Groundwater Isoscapes in a Montane Headwater Catchment Show Dominance of Well-Mixed Storage. *Hydrol Process* **2017**, *31* (20), 3504–3519. https://doi.org/https://doi.org/10.1002/hyp.11271.

(64) Gong, G.; Mattevada, S.; O'Bryant, S. E. Comparison of the Accuracy of Kriging and IDW Interpolations in Estimating Groundwater Arsenic Concentrations in Texas. *Environ Res* **2014**, *130*, 59–69. https://doi.org/https://doi.org/10.1016/j.envres.2013.12.005.

(65) Tayyab, M.; Aslam, R. A.; Farooq, U.; Ali, S.; Khan, S. N.; Iqbal, M.; Khan, M. I.; Saddique, N. Comparative Study of Geospatial Techniques for Interpolating Groundwater Quality Data in Agricultural Areas of Punjab, Pakistan. *Water (Basel)* **2024**, *16* (1). https://doi.org/10.3390/w16010139.

(66) Shi, Y.; Li, L.; Zhang, L. Application and Comparing of IDW and Kriging Interpolation in Spatial Rainfall Information. In *Proc.SPIE*; 2007; Vol. 6753, p 67531I. https://doi.org/10.1117/12.761859.

(67) OuYang, D.; Feng, H.-Y. Reconstruction of 2D Polygonal Curves and 3D Triangular Surfaces via Clustering of Delaunay Circles/Spheres. *Computer-Aided Design* **2011**, *43* (8), 839–847. https://doi.org/https://doi.org/10.1016/j.cad.2011.04.003.

(68) Syakur, M. A.; Khotimah, B. K.; Rochman, E. M. S.; Satoto, B. D. Integration K-Means Clustering Method and Elbow Method for Identification of the Best Customer Profile Cluster. In *IOP Conference Series: Materials Science and Engineering*; Institute of Physics Publishing, 2018; Vol. 336. https://doi.org/10.1088/1757-899X/336/1/012017.

(69) Rousseeuw, P. J. Silhouettes: A Graphical Aid to the Interpretation and Validation of Cluster Analysis. *J Comput Appl Math* **1987**, *20*, 53–65. https://doi.org/https://doi.org/10.1016/0377-0427(87)90125-7.
(70) Meng, S. X.; Maynard, J. B. Use of Statistical Analysis to Formulate Conceptual Models of Geochemical Behavior: Water Chemical Data from the Botucatu Aquifer in São Paulo State, Brazil. *J Hydrol (Amst)* **2001**, *250* (1), 78–97. https://doi.org/https://doi.org/10.1016/S0022-1694(01)00423-1.
(71) Helena, B.; Pardo, R.; Vega, M.; Barrado, E.; Fernandez, J. M.; Fernandez, L. Temporal Evolution of Groundwater Composition in an Alluvial Aquifer (Pisuerga River, Spain) by Principal Component Analysis. *Water Res* **2000**, *34* (3), 807–816. https://doi.org/https://doi.org/10.1016/S0043-1354(99)00225-0.
(72) Singh, K. P.; Malik, A.; Mohan, D.; Sinha, S. Multivariate Statistical Techniques for the Evaluation of Spatial and Temporal Variations in Water Quality of Gomti River (India)—a Case Study. *Water Res* **2004**, *38* (18), 3980–3992. https://doi.org/https://doi.org/10.1016/j.watres.2004.06.011.
(73) Güler, C.; Thyne, G. D.; McCray, J. E.; Turner, K. A. Evaluation of Graphical and Multivariate Statistical Methods for Classification of Water Chemistry Data. *Hydrogeol J* **2002**, *10* (4), 455–474. https://doi.org/10.1007/s10040-002-0196-6.
(74) Johnson, T. D.; Belitz, K. Domestic Well Locations and Populations Served in the Contiguous U.S.: 1990. *Science of The Total Environment* **2017**, *607–608*, 658–668. https://doi.org/https://doi.org/10.1016/j.scitotenv.2017.07.018.
(75) Brennecka, G. A.; Borg, L. E.; Hutcheon, I. D.; Sharp, M. A.; Anbar, A. D. Natural Variations in Uranium Isotope Ratios of Uranium Ore Concentrates: Understanding the 238U/235U Fractionation Mechanism. *Earth Planet Sci Lett* **2010**, *291* (1), 228–233. https://doi.org/https://doi.org/10.1016/j.epsl.2010.01.023.
(76) Uvarova, Y. A.; Kyser, T. K.; Geagea, M. L.; Chipley, D. Variations in the Uranium Isotopic Compositions of Uranium Ores from Different Types of Uranium Deposits. *Geochim Cosmochim Acta* **2014**, *146*, 1–17. https://doi.org/https://doi.org/10.1016/j.gca.2014.09.034.
(77) Bopp IV, C. J.; Lundstrom, C. C.; Johnson, T. M.; Glessner, J. J. G. Variations in 238U/235U in Uranium Ore Deposits: Isotopic Signatures of the U Reduction Process? *Geology* **2009**, *37* (7), 611–614. https://doi.org/10.1130/G25550A.1.
(78) Wang, X.; Johnson, T. M.; Lundstrom, C. C. Isotope Fractionation during Oxidation of Tetravalent Uranium by Dissolved Oxygen. *Geochim Cosmochim Acta* **2015**, *150*, 160–170. https://doi.org/https://doi.org/10.1016/j.gca.2014.12.007.
(79) Clark, S. K.; Johnson, T. M. Selenium Stable Isotope Investigation into Selenium Biogeochemical Cycling in a Lacustrine Environment: Sweitzer Lake, Colorado. *J Environ Qual* **2010**, *39* (6), 2200–2210. https://doi.org/https://doi.org/10.2134/jeq2009.0380.
(80) Raddatz, A. L.; Johnson, T. M.; McLing, T. L. Cr Stable Isotopes in Snake River Plain Aquifer Groundwater: Evidence for Natural Reduction of Dissolved Cr(VI). *Environ Sci Technol* **2011**, *45* (2), 502–507. https://doi.org/10.1021/es102000z.
(81) Williams, K. H.; Long, P. E.; Davis, J. A.; Wilkins, M. J.; N'Guessan, A. L.; Steefel, C. I.; Yang, L.; Newcomer, D.; Spane, F. A.; Kerkhof, L. J.; Mcguinness, L.; Dayvault, R.;

Lovley, D. R. Acetate Availability and Its Influence on Sustainable Bioremediation of Uranium-Contaminated Groundwater. *Geomicrobiol J* **2011**, *28* (5–6), 519–539. https://doi.org/10.1080/01490451.2010.520074.

(82) Long, P. E.; Williams, K. H.; Davis, J. A.; Fox, P. M.; Wilkins, M. J.; Yabusaki, S. B.; Fang, Y.; Waichler, S. R.; Berman, E. S. F.; Gupta, M.; Chandler, D. P.; Murray, C.; Peacock, A. D.; Giloteaux, L.; Handley, K. M.; Lovley, D. R.; Banfield, J. F. Bicarbonate Impact on U(VI) Bioreduction in a Shallow Alluvial Aquifer. *Geochim Cosmochim Acta* **2015**, *150*, 106–124. https://doi.org/https://doi.org/10.1016/j.gca.2014.11.013.

(83) Newsome, L.; Morris, K.; Lloyd, J. R. The Biogeochemistry and Bioremediation of Uranium and Other Priority Radionuclides. *Chem Geol* **2014**, *363*, 164–184. https://doi.org/https://doi.org/10.1016/j.chemgeo.2013.10.034.

(84) Masue, Y.; Loeppert, R. H.; Kramer, T. A. Arsenate and Arsenite Adsorption and Desorption Behavior on Coprecipitated Aluminum:Iron Hydroxides. *Environ Sci Technol* **2007**, *41* (3), 837–842. https://doi.org/10.1021/es061160z.

(85) Davis, K. W.; Putnam, L. D.; LaBelle, A. R. *Scientific Investigations Report 2014-5241 Prepared in Cooperation with the Oglala Sioux Tribe Conceptual and Numerical Models of Groundwater Flow in the Ogallala*.

(86) Scanlon, B. R.; Nicot, J. P.; Reedy, R. C.; Kurtzman, D.; Mukherjee, A.; Nordstrom, D. K. Elevated Naturally Occurring Arsenic in a Semiarid Oxidizing System, Southern High Plains Aquifer, Texas, USA. *Applied Geochemistry* **2009**, *24* (11), 2061–2071. https://doi.org/https://doi.org/10.1016/j.apgeochem.2009.08.004.

(87) Bhattacharya, P.; Claesson, M.; Bundschuh, J.; Sracek, O.; Fagerberg, J.; Jacks, G.; Martin, R. A.; Storniolo, A. del R.; Thir, J. M. Distribution and Mobility of Arsenic in the Río Dulce Alluvial Aquifers in Santiago Del Estero Province, Argentina. *Science of The Total Environment* **2006**, *358* (1), 97–120. https://doi.org/https://doi.org/10.1016/j.scitotenv.2005.04.048.

(88) Smedley, P. L.; Kinniburgh, D. G. A Review of the Source, Behaviour and Distribution of Arsenic in Natural Waters. *Applied Geochemistry* **2002**, *17* (5), 517–568. https://doi.org/https://doi.org/10.1016/S0883-2927(02)00018-5.

(89) Golubev, V. N.; Chernyshev, I. V; Kochkin, B. T.; Tarasov, N. N.; Ochirova, G. V; Chugaev, A. V. Uranium Isotope Variations ($^{234}U/^{238}U$ and $^{238}U/^{235}U$) and Behavior of U-Pb Isotope System in the Vershinnoe Sandstone-Type Uranium Deposit, Vitim Uranium Ore District, Russia. *Journal of Earth Science* **2022**, *33* (2), 317–324. https://doi.org/10.1007/s12583-021-1436-9.

(90) Meunier, J. D. *Uranium Mobility in the Sediment-Hosted Uranium Deposit of Coutras, France*; 1992; Vol. 7.

(91) Golubev, V. N.; Tarasov, N. N.; Chernyshev, I. V; Chugaev, A. V; Ochirova, G. V; Kochkin, B. T. Post-Ore Processes of Uranium Migration in the Sandstone-Hosted Type Deposits: 234U/238U, 238U/235U and U–Pb Systematics of Ores of the Namaru Deposit, Vitim District, Northern Transbaikalia. *Geology of Ore Deposits* **2021**, *63* (4), 287–299. https://doi.org/10.1134/S1075701521040024.

(92) Davis, K. W.; Putnam, L. D.; LaBelle, A. R.; Survey, U. S. G. *Conceptual and Numerical Models of Groundwater Flow in the Ogallala and Arikaree Aquifers, Pine Ridge Indian*

Reservation Area, South Dakota, Water Years 1980-2009; Reston, VA, 2015. https://doi.org/10.3133/sir20145241.

(93) Weyer, S.; Anbar, A. D.; Gerdes, A.; Gordon, G. W.; Algeo, T. J.; Boyle, E. A. Natural Fractionation of 238U/235U. *Geochim Cosmochim Acta* **2008**, *72* (2), 345–359. https://doi.org/https://doi.org/10.1016/j.gca.2007.11.012.

(94) Bopp, C. J. I. V; Lundstrom, C. C.; Johnson, T. M.; Sanford, R. A.; Long, P. E.; Williams, K. H. Uranium 238U/235U Isotope Ratios as Indicators of Reduction: Results from an in Situ Biostimulation Experiment at Rifle, Colorado, U.S.A. *Environ Sci Technol* **2010**, *44* (15), 5927–5933. https://doi.org/10.1021/es100643v.

(95) Shiel, A. E.; Laubach, P. G.; Johnson, T. M.; Lundstrom, C. C.; Long, P. E.; Williams, K. H. No Measurable Changes in 238U/235U Due to Desorption–Adsorption of U(VI) from Groundwater at the Rifle, Colorado, Integrated Field Research Challenge Site. *Environ Sci Technol* **2013**, *47* (6), 2535–2541. https://doi.org/10.1021/es303913y.

(96) Basu, A.; Sanford, R. A.; Johnson, T. M.; Lundstrom, C. C.; Löffler, F. E. Uranium Isotopic Fractionation Factors during U(VI) Reduction by Bacterial Isolates. *Geochim Cosmochim Acta* **2014**, *136*, 100–113. https://doi.org/https://doi.org/10.1016/j.gca.2014.02.041.

(97) Brown, S. T.; Basu, A.; Ding, X.; Christensen, J. N.; DePaolo, D. J. Uranium Isotope Fractionation by Abiotic Reductive Precipitation. *Proc Natl Acad Sci U S A* **2018**, *115* (35), 8688–8693. https://doi.org/10.1073/pnas.1805234115.

(98) Stylo, M.; Neubert, N.; Wang, Y.; Monga, N.; Romaniello, S. J.; Weyer, S.; Bernier-Latmani, R. Uranium Isotopes Fingerprint Biotic Reduction. *Proceedings of the National Academy of Sciences* **2015**, *112* (18), 5619–5624. https://doi.org/10.1073/pnas.1421841112.

(99) Stirling, C. H.; Andersen, M. B.; Warthmann, R.; Halliday, A. N. Isotope Fractionation of 238U and 235U during Biologically-Mediated Uranium Reduction. *Geochim Cosmochim Acta* **2015**, *163*, 200–218. https://doi.org/https://doi.org/10.1016/j.gca.2015.03.017.

(100) Jemison, N. E.; Shiel, A. E.; Johnson, T. M.; Lundstrom, C. C.; Long, P. E.; Williams, K. H. Field Application of 238U/235U Measurements To Detect Reoxidation and Mobilization of U(IV). *Environ Sci Technol* **2018**, *52* (6), 3422–3430. https://doi.org/10.1021/acs.est.7b05162.

(101) Martin, J. E. ,; Sawyer, J. F. ,; Fahrenbach, M. D. ,; Tomhave, D. W. ,; Schulz, L. D. *Geologic Map of South Dakota*; 2004.

Supplementary Information for

ISOSCAPES as a Regional-Scale Lens on Understanding the Groundwater Uranium Cycling in the Northern Plains Aquifer

Authors: *Arijeet Mitra[1], Randall Hughes[2], Tracy Zacher[2], Rae O'Leary[2], Bayley Sbardellati[3], Mason Stahl[3], Reno Red Cloud[4], Shams Azad[5], James Ross[5], Ben Bostick[5], Steve Chillrud[5], Alex N. Halliday[5], Ana Navas-Acien[1], Kathrin Schilling[1], Anirban Basu[1]*

Author details: [1]Mailman School of Public Health, Columbia University, New York, NY 10032, [2]Missouri Breaks Industries Research Inc, Eagle Butte, SD 57625, [3]Environmental Science Policy and Engineering, Union College, 807 Union Street, Schenectady, NY 12308, [4]Oglala Sioux Tribe Water Resources, Pine Ridge, SD 57770, [5]Lamont Doherty Earth Observatory, Columbia University, 61 Route 9W, Palisades, NY 10964

***Corresponding address:** am6368@cumc.columbia.edu

S1. SITE DESCRIPTION

Our study area lies within the northern Great Plains and is underlain by Cenozoic sedimentary deposits that host naturally occurring U) and mineralization. The region's stratigraphy is primarily composed of the White River Group (Oligocene) and Arikaree Group (Miocene), which contain U deposits that contribute to groundwater geochemistry. The depositional history, lithology, and mineral composition of these units play a crucial role in controlling U occurrence, mobility, and transport in the aquifer. White River Group consists of the Chamberlain Pass and Chadron Formations, both of which contain U in the form of roll front deposit tuffaceous sandstones (Fig S2).[19] These deposits are associated with secondary U minerals such as uraninite and coffinite, which can dissolve under oxidizing conditions, releasing U into groundwater. Additionally, previous studies have documented roll-front type U mineralization in paleochannel deposits within the White River Group, indicating that groundwater flow has historically influenced U deposition and remobilization. Arikaree Group, overlying the White River Group, the Arikaree Formation serves as the primary aquifer for domestic water supply in the study area. The basal Rockyford Ash Zone, a distinct tuffaceous interval, is particularly relevant due to its fine-grained ash composition and elevated trace metal content. Although this zone does not contain economically viable U concentrations, it can still influence U and As mobilization due to the change in redox condition of the aquifer condition, which alters over time and releases trace elements into groundwater. The Arikaree aquifer is the main water-bearing unit, with groundwater flow generally from south to north. Due to the low regional dip (<1°), groundwater movement is slow and topographically driven, with recharge occurring primarily from precipitation and snowmelt infiltration. Groundwater pathways in the study area are influenced by buried paleochannels within the White River Group, which act as preferential flow conduits. These features have been identified as key zones where U may have been historically deposited and later remobilized, affecting present-day U distributions in the aquifer system. The interaction of groundwater with U-bearing volcanic ash deposits and bentonite clays leads to variable U concentrations, dependent on both mineral solubility and redox conditions. The study area has a semi-arid climate, with low annual precipitation and recurrent droughts. The landscape consists predominantly of prairie grasslands, interspersed with sandstone buttes in the south

and badland formations in the north. Due to limited rainfall and periodic water scarcity, much of the land is unsuitable for conventional agriculture, though grasslands support extensive cattle ranching.

S2. SAMPLE COLLECTION

Groundwater samples were collected from private in 141 locations across Shannon, Jackson, and Bennett counties. The coordinates for the sampling sites were recorded using in-built GPS present in IPAD and further crosschecked using their physical address. None of the samples were taken from abandoned wells or observation wells. The groundwater samples were collected from spigots of private wells located on residential premises of local native American communities, which they use for domestic purposes. Each well was sampled for major anions concentration, trace elements concentration, and U isotopes. Prior to sampling, each well was purged following the standard sampling protocol until the field parameters (e.g., temperature, pH, Eh, EC) are collected. On-site measurements of temperature, pH, redox potential (Eh), and electrical conductivity (EC) were performed during sampling. It is noteworthy to mention that the introduction of oxygen (O_2) during sample collection can alter these measurements, making them less accurate and leading to misleading Eh-pH values. Therefore, the interpretation of redox condition presented here is focused mainly on the concentration of anion, cations and U isotope ratios. We imputed missing field parameter data using the Delaunay triangulation method, a widely accepted standard in groundwater studies for handling missing values. The water samples were filtered using 0.22 μm cellulose acetate membrane filters (Millipore) to remove suspended particles and stored in pre-cleaned borosilicate glass and HDPE bottles. The samples for trace element analysis and U isotopes were acidified with double distilled nitric acid up to 0.13M to prevent biological activity and the precipitation of metals. Finally, they were refrigerated until trace element and U isotope analysis. The samples for anions were filtered and refrigerated without acidification.

S3. TRACE ELEMENT and ANION CONCENTRATION ANALYSIS

Trace metal analyses were performed on a double-focusing sector-field inductively coupled plasma-mass spectrometer (Thermo Element XR) with high-resolution present at the Lamont-Doherty Earth Observatory,

Columbia University. This instrument has three resolutions – elements were run in the most appropriate resolution based on spectral interferences and sensitivity. Samples were acidified with concentrated HNO3 to 0.16N. Optima grade HNO3 was used throughout. For analysis, samples were diluted with 5ppb Indium (In, the internal standard) in 0.16 N HNO3 by a factor of 10 (200 µL to 1800 µL). Standard curves were prepared by diluting primary mixed-standard in-house stock solutions with the Indium (In) solution in the same manner. Sample concentrations were determined after correction for the internal standard. Blank correction was done by subtracting the value of clean 0.16N HNO3 diluted in the In solution in the same manner. Anions were analyzed on a Dionex ICS-2100 at Union College. Five-point calibration curves for F, Cl, Br, NO2, NO3, SO4, and PO4 were developed for each instrument run and known reference waters were analyzed at the start, middle, and end of each run to ensure instrument accuracy and confirm that there was no appreciable instrument drift over the course of a run.

S4. U ISOTOPIC ANALYSIS

For isotopic measurements, a double isotope spike (IRMM 3636a, ^{236}U: $^{233}U = 1.01906$) was used to correct for isotopic fractionation during sample purification and mass spectrometry. [32,93–96] Prior to purification, an aliquot of the double spike solution was added to each sample containing approximately 50 ng of U to attain a ^{238}U to ^{236}U ratio of about 20. The spiked samples were then evaporated to complete dryness, re-dissolved in 1 mL of 3N HNO_3 and purified using the UTEVA resin (Eichrom). U(VI) in the samples bounds to the resin and all cations and thorium were eluted using a combination of 4 mL of 3N HNO_3 and 1 mL of concentrated hydrochloric acid (HCl). Then U (VI) was eluted from the resin with 2.4mL of 0.05N HCl solution. The purified samples were dried completely and treated with a few drops of concentrated HNO_3 to remove organic residues from the purification process. U isotope measurements were carried out using a third generation Nu Plasma 3 MC-ICP-MS (Wrexham, UK) operating in low-resolution mode housed at NICER Lab, Columbia University. Purified samples were introduced to the instrument as 0.13M (or 2%) HNO_3 solutions via an Aridus 3 CETAC desolvating nebulizer. The $^{233}U/^{236}U$, $^{234}U/^{236}U$, $^{235}U/^{236}U$, $^{234}U/^{238}U$, and $^{238}U/^{236}U$ ratios were measured simultaneously. Precise $^{238}U/^{235}U$ ratios were obtained by correcting for the instrumental mass bias using a double-spike analysis method described in references [58].

The U isotope standard CRM 145 was analyzed after every 2 samples as bracketing standards to monitor and correct for any drift.

S5. CLUSTER ANALYSIS: DETAILED IMPLEMENTATION & VALIDATION

Z-score normalization was applied to standardize numerical variables:

$$Z = \frac{(\mathrm{X} - \mu)}{\sigma}$$

where Z represents the standardized value, X is the original variable, μ is the mean, and σ is the standard deviation. To determine the optimal cluster number, the Elbow Method was used by calculating the Within-Cluster Sum of Squares (WSS):

$$WSS = \sum_{i=1}^{k} \sum_{x \in C_i} \| x - \mu_i \|$$

where C_i denotes a cluster, μ_i is its centroid, and x is an individual data point. The Silhouette Score, which evaluates clustering performance, is expressed as:

$$S(i) = \frac{b(i) - a(i)}{\max(a(i), b(i))}$$

where *S(i)* is the silhouette coefficient for sample *i*, *a(i)* is the mean intra-cluster distance, and *b(i)* is the mean nearest-cluster distance. The highest silhouette score indicated the optimal number of clusters, ensuring well-separated and internally cohesive groupings [69]. Clustering was performed over a range of k = 2 to 10, and the final K-means clustering results were visualized using a scatter plot. Hierarchical clustering (Ward's method) was also performed to validate K-means results. The Ward's method distance metric is given by:

$$D(A,B) = \frac{|A||B|}{|A| + |B|} \parallel \mu_A - \mu_B \parallel^2$$

where *D(A, B)* represents the distance between clusters A and B. |A| and |B| are the number of points in each cluster, and μ_A and μ_B are their respective centroids. A dendrogram based on Euclidean distance illustrated hierarchical relationships between groundwater samples, providing insights into sample similarity and natural divisions within the dataset. Box plots (Figures S11-14) compare geochemical variability between clusters.

S6. PCA: ADDITIONAL STATISTICAL INSIGHTS

PCA was applied to identify dominant geochemical drivers of U variability. Seven-component PCA was initially conducted, with the explained variance ratio used to determine significant PCs. A cumulative variance plot (Figure S15) showed that PC1 and PC2 accounted for ~70% of dataset variance, justifying dimensionality reduction. The biplot (Figure 5) illustrates PC1 and PC2 loadings for geochemical variables, where the arrow length and direction indicate the contribution of each variable to the principal components. The PCA loading table provides numerical contributions of each variable to PC1 and PC2.

Table S1: Expected process-related isotope signature of U in water samples

Reaction	Pathway	ε (^{238}U) ‰	Isotopic enrichment in water sample	δ^{238}U (‰)	References
Reduction	Abiotic	0.8	Large ^{235}U enrichment	negative	[97]
Reduction	Biotic	0.72 to 0.99	Large ^{235}U enrichment	negative	[37,59,98,99]
Adsorption	Mineral Phases	-0.15	Small ^{238}U enrichment	positive	[38,39]
Dissolution			Large ^{238}U enrichment	positive	[100]

Table S2: Details of field parameters and trace element concentration measured for the groundwater samples of this study. The units for each parameter are listed below.

Sample ID	pH	Eh	EC	NO_3^-	SO_4^{2-}	F	Cl	Fe	Mn	Se	V	As
		mV	µS/cm	mg/L	mg/L	mg/L	mg/L	µg/L	µg/L	µg/L	µg/L	µg/L
Cluster 1	7.70	408.00	287.00	6.61	8.77	0.50	2.65	13.56	9.46	19.90	0.04	0.28
	7.60	425.00	315.00	7.49	30.42	0.18	1.53	0.12	1.61	3.85	106.55	3.07
	7.80	428.80	337.30	8.06	15.77	0.35	6.33	1.10	41.35	8.45	58.82	4.41
	7.70	390.00	348.00	4.25	10.40	0.33	1.91	0.14	1.23	6.25	20.29	16.41
	7.60	421.00	365.00	104.18	37.93	0.28	37.56	0.08	0.76	0.60	16.48	12.09
	7.60	416.00	638.00	4.61	24.75	0.30	4.11	0.75	0.16	7.29	12.06	10.15
	7.50	374.00	542.00	2.28	5.84	0.40	2.28	0.27	5.08	15.42	12.00	11.06
	7.60	408.00	418.00	2.99	33.78	0.42	7.23	0.31	1.22	6.45	25.75	7.28
	7.00	316.00	596.00	1.14	79.17	0.66	11.46	2.60	0.40	7.06	12.70	14.69
	7.40	371.00	315.00	8.26	17.96	0.27	15.39	0.00	0.19	3.68	15.79	14.02
	7.30	373.00	691.00	2.89	23.73	0.39	13.11	6.17	0.79	5.09	23.94	18.44
	7.30	380.50	588.90	16.57	33.39	0.30	11.06	0.80	0.44	8.63	10.02	11.30
	7.20	381.00	593.00	11.33	28.46	0.46	22.49	0.00	0.22	10.61	39.76	23.02
	7.50	505.00	605.00	2.09	50.84	0.38	8.07	2.09	0.04	9.37	12.97	14.96
	8.50	440.00	753.00	2.03	46.52	0.30	6.81	1.40	0.26	7.51	11.51	11.71
	7.60	395.00	386.00	2.83	39.11	0.47	15.02	2.92	0.41	5.90	37.66	24.82
	7.70	548.00	190.00	2.81	23.19	0.48	3.73	3.38	0.39	3.17	24.48	10.94
	7.50	400.00	416.00	8.85	38.96	0.43	7.56	2.98	0.36	8.15	33.79	19.41
	7.70	412.00	530.00	0.00	99.76	0.29	67.45	5.08	0.27	15.42	12.00	11.06
Min	**7.00**	**316.00**	**190.00**	**0.00**	**5.84**	**0.18**	**1.53**	**0.00**	**0.04**	**0.60**	**0.04**	**0.28**
Max	8.50	548.00	753.00	104.18	99.76	0.66	67.45	13.56	41.35	19.90	106.55	24.82
Median	**7.60**	**408.00**	**418.00**	**4.25**	**30.42**	**0.38**	**7.56**	**1.10**	**0.41**	**7.29**	**16.48**	**11.71**
Cluster 2												
	7.40	765.00	524.00	5.90	8.77	0.29	4.12	26.80	507.70	0.08	0.06	0.28
	7.40	378.00	632.00	1.67	21.30	0.13	2.33	40.41	892.50	0.02	0.01	0.11
	7.70	407.00	348.00	1.83	15.36	0.56	0.79	42.95	873.27	0.02	0.01	0.12
	7.60	367.70	747.00	0.00	108.95	0.34	18.01	25.53	228.38	0.01	0.01	0.39
	7.60	393.80	765.00	9.81	117.49	0.39	13.84	30.17	322.16	0.01	0.01	0.04
	7.70	451.00	429.00	9.16	38.15	0.33	20.23	26.52	492.37	0.01	0.02	0.07
	7.50	469.70	530.90	5.39	78.51	0.21	7.87	28.79	997.19	0.05	0.01	0.13
	7.40	424.60	816.10	20.83	518.85	0.27	128.52	6.64	5.96	0.41	0.05	0.15
	7.70	412.00	530.00	5.80	73.40	0.26	4.28	26.11	716.68	0.00	0.02	0.10
	7.80	479.00	911.00	0.34	249.35	0.77	31.52	107.80	400.79	0.00	0.01	0.33
	7.70	409.00	315.00	12.25	65.70	0.24	79.65	752.20	1.61	1.17	10.67	9.92
	7.30	379.20	579.50	0.01	83.97	0.31	17.06	316.04	688.24	0.00	0.14	3.58

	7.90	329.00	585.00	0.01	219.28	0.17	9.27	24.19	365.25	0.11	10.05	5.45
	7.50	414.00	451.00	0.35	242.01	0.74	31.43	0.57	0.22	0.71	0.05	0.30
	8.10	391.00	778.00	0.79	282.53	0.11	31.29	6.14	14.96	0.69	0.08	0.40
	7.60	402.00	524.00	0.00	219.28	0.17	9.27	24.19	365.25	0.11	10.05	5.45
Min	**7.30**	**329.00**	**315.00**	**0.00**	**8.77**	**0.11**	**0.79**	**0.57**	**0.22**	**0.00**	**0.01**	**0.04**
Max	8.10	765.00	911.00	20.83	518.85	0.77	128.52	752.20	997.19	1.17	10.67	9.92
Median	**7.60**	**408.00**	**555.20**	**1.75**	**96.46**	**0.28**	**15.45**	**26.66**	**383.02**	**0.04**	**0.04**	**0.29**
Cluster 3												
	7.60	435.00	273.00	3.23	22.86	0.40	2.72	45.18	2.55	0.04	0.06	0.06
	7.00	367.00	474.00	0.20	13.14	0.53	2.41	75.14	463.15	0.03	0.03	0.07
	7.50	425.00	315.00	2.20	10.71	0.57	1.47	30.57	175.48	0.03	0.06	0.07
	7.60	402.00	421.00	4.24	13.37	0.40	8.58	72.10	166.67	0.09	0.01	0.22
	7.60	402.00	524.00	2.93	18.44	0.25	1.90	2.04	0.12	0.88	8.45	6.69
	7.60	402.00	524.00	2.84	13.96	0.39	1.11	15.51	186.69	0.00	0.11	0.07
	7.70	451.00	429.00	7.31	35.17	0.38	4.53	46.51	252.05	0.06	0.01	0.13
	7.80	425.00	311.00	4.79	8.88	0.30	1.54	8.83	5.84	0.84	0.09	0.31
	7.60	368.60	380.60	5.46	2.48	0.29	3.46	11.42	40.65	0.01	0.04	0.08
	8.00	430.00	686.00	1.46	121.77	0.53	10.29	59.16	0.98	0.31	0.02	0.08
	7.70	416.00	410.00	1.69	31.33	0.37	2.33	95.12	159.86	0.01	0.02	0.16
	7.20	353.00	384.00	3.25	10.46	0.44	2.27	37.21	427.32	0.00	0.02	0.07
	7.70	419.70	342.30	17.10	10.29	0.18	9.55	9.40	35.64	0.02	0.55	0.42
	7.60	434.00	393.00	18.84	7.35	0.18	4.07	10.68	60.92	0.20	1.05	0.96
	7.80	414.00	353.00	0.16	12.72	0.52	2.13	47.92	339.64	0.01	0.02	0.06
	7.60	396.70	528.20	6.06	48.55	0.24	4.84	16.05	2.15	2.88	0.10	0.19
	7.50	432.00	404.80	5.69	7.27	0.51	2.76	56.15	286.95	0.12	0.02	0.02
	7.50	373.00	523.00	2.63	8.08	0.36	4.79	0.15	2.26	3.14	23.47	8.25
	7.90	426.00	306.00	6.99	34.21	0.35	1.61	0.06	3.51	0.89	5.39	6.09
	8.00	431.00	384.00	2.64	17.91	0.61	0.77	0.29	1.34	0.62	10.11	3.26
	8.10	433.00	279.00	30.23	16.14	0.32	9.96	0.49	0.34	0.03	0.01	1.44
	7.60	420.00	502.00	6.12	35.11	0.34	2.29	2.70	1.69	2.07	9.20	11.50
	7.70	418.00	371.00	4.29	11.65	0.37	1.54	205.83	18.23	0.02	3.53	10.87
	7.60	432.00	710.00	5.82	12.38	0.32	1.58	0.07	0.00	1.11	11.62	8.32
	7.70	429.00	369.00	2.45	10.93	0.41	2.17	10.12	0.00	0.78	10.59	8.19
	7.60	393.00	385.00	2.35	12.27	0.41	2.32	0.10	0.78	1.49	7.12	5.42
	7.60	393.00	385.00	16.84	44.10	0.49	10.09	0.12	2.04	0.88	8.45	6.69
	8.10	374.00	691.00	1.68	18.25	0.52	1.00	0.03	0.00	1.08	10.89	8.70
	7.60	397.00	339.00	2.73	12.61	0.62	2.48	0.41	0.42	0.48	0.04	0.24
	7.70	397.00	334.00	9.70	32.15	0.57	9.77	0.12	0.82	1.43	9.08	7.22
	7.70	410.00	408.00	2.19	4.01	0.34	1.22	0.68	6.25	1.94	12.68	6.49
	7.60	400.00	343.00	4.02	8.21	0.34	2.36	0.22	1.46	0.20	13.97	13.03

7.80	383.00	334.00	4.97	6.50	0.47	4.19	0.07	1.45	1.09	7.50	8.99
7.20	379.00	723.00	0.92	37.37	0.28	9.81	0.09	0.53	0.19	7.34	2.89
6.80	345.00	689.00	6.87	24.46	0.32	4.91	0.31	1.92	1.50	10.93	5.19
8.40	419.00	720.00	1.50	14.14	0.50	0.92	0.45	0.69	4.27	27.12	6.96
7.80	405.00	334.00	0.30	115.87	2.25	10.53	0.81	3.05	0.00	3.13	2.90
7.30	380.50	588.90	1.35	13.98	0.58	1.23	0.12	1.80	0.70	6.08	6.31
7.40	410.00	330.00	6.80	39.20	0.49	2.26	154.87	9.81	0.17	6.69	24.41
8.10	412.00	630.00	1.40	7.21	0.37	1.61	1.81	0.11	0.65	11.76	9.08
7.60	400.70	333.40	1.16	10.68	0.51	1.74	0.07	0.04	0.32	13.63	13.29
7.40	360.00	784.00	2.20	29.14	0.31	4.92	0.00	0.03	2.41	6.12	7.32
7.20	319.20	593.30	2.50	34.02	0.32	2.38	2.36	0.02	0.92	6.57	7.13
7.80	383.00	410.00	4.92	16.36	0.54	7.22	0.95	0.06	2.57	5.69	5.11
7.30	330.00	352.00	0.00	22.54	0.33	4.89	5.55	0.06	1.12	7.18	5.41
7.50	331.00	373.00	0.00	21.37	0.17	2.55	2.83	0.08	2.37	6.08	4.38
7.40	324.00	498.00	3.68	42.49	0.34	10.02	10.77	2.46	2.97	5.69	6.76
7.20	349.00	642.00	0.00	21.85	0.46	6.83	0.39	0.28	1.43	6.28	11.69
6.20	339.00	433.00	3.03	38.90	0.39	9.10	2.69	0.33	3.36	5.74	6.17
7.20	381.00	593.00	8.95	29.27	0.37	0.95	5.65	0.30	0.75	7.07	4.21
7.00	367.00	474.00	2.73	4.41	0.40	1.43	1.78	0.15	0.41	13.14	7.06
7.40	314.00	312.00	10.54	5.97	0.57	1.37	4.61	0.26	0.35	17.18	10.32
8.40	436.00	327.00	4.11	36.47	0.40	2.95	0.76	0.21	1.39	5.37	4.16
7.60	342.00	392.00	3.82	21.04	0.45	3.08	4.38	0.20	0.95	18.86	12.08
7.40	378.00	632.00	7.49	30.42	0.18	1.53	1.19	0.04	0.88	6.40	4.02
7.50	432.00	404.80	0.00	47.70	0.46	14.71	4.75	0.13	0.53	5.50	7.72
7.60	394.00	779.00	1.31	10.52	0.57	1.02	2.64	0.09	0.68	10.92	13.35
7.50	505.00	605.00	3.34	39.94	0.35	3.32	8.06	0.43	1.79	6.30	7.43
7.70	396.00	411.80	5.02	4.73	0.33	0.93	0.00	0.15	0.34	8.81	2.53
7.80	377.00	273.00	17.90	13.58	0.40	16.83	1.83	0.25	2.72	13.80	8.44
8.50	440.00	753.00	2.62	19.56	0.47	3.46	1.63	0.12	4.97	7.14	7.61
7.50	400.00	416.00	3.68	42.49	0.34	10.02	10.77	2.46	2.97	5.69	6.76
7.00	316.00	596.00	3.24	5.23	0.25	1.94	0.00	0.17	0.49	8.35	4.64
7.40	371.00	315.00	6.48	52.04	0.56	2.36	1.81	0.30	1.76	5.30	9.84
7.70	339.10	557.40	2.49	20.70	0.28	1.40	0.36	0.03	0.12	5.27	3.87
8.10	277.00	355.00	0.00	47.26	0.40	10.60	18.70	0.39	0.12	4.09	5.97
7.10	412.00	733.00	2.17	13.17	0.60	4.53	4.53	0.15	1.89	8.90	5.81
7.90	387.00	346.00	1.76	10.33	0.56	3.17	9.27	0.60	0.38	5.44	5.09
7.10	422.00	744.00	7.26	26.97	0.35	2.36	0.12	0.02	2.74	7.92	5.05
7.40	431.20	616.20	13.75	33.07	0.27	5.52	0.98	0.03	3.76	6.74	4.88
7.40	431.20	616.20	3.02	9.48	0.34	2.12	1.40	0.02	0.51	9.41	3.88
7.40	426.00	846.00	2.63	8.08	0.36	4.79	8.70	0.39	1.56	10.47	5.82

	8.10	405.00	425.00	5.29	20.17	0.24	2.62	1.91	0.43	1.98	7.68	4.22
	8.00	414.00	420.00	2.62	19.56	0.47	3.46	1.63	0.12	4.97	7.14	7.61
	7.50	326.00	554.00	0.82	22.21	0.27	3.18	0.00	10.12	0.78	10.59	8.19
	7.60	442.00	407.00	0.01	53.31	0.28	7.60	2.16	32.64	0.69	2.34	7.24
	7.30	435.00	927.00	8.11	13.95	0.38	0.78	18.65	3.83	0.74	6.53	4.98
	8.00	458.00	360.00	0.00	83.59	0.84	7.20	3.22	1.25	0.00	0.37	8.25
	7.70	395.00	735.00	2.58	30.26	0.43	3.67	1.80	0.12	0.70	6.08	6.31
	7.60	442.00	407.00	1.83	10.27	0.53	1.39	0.42	0.41	0.48	0.04	0.24
Min	**6.20**	**277.00**	**273.00**	**0.00**	**2.48**	**0.17**	**0.77**	**0.00**	**0.00**	**0.00**	**0.01**	**0.02**
Max	8.50	505.00	927.00	30.23	121.77	2.25	16.83	205.83	463.15	4.97	27.12	24.41
Median	**7.60**	**401.35**	**413.90**	**2.98**	**18.34**	**0.39**	**2.67**	**1.98**	**0.48**	**0.75**	**6.35**	**5.82**
Cluster 4												
	7.50	373.00	523.00	7.39	16.77	0.40	5.42	127.85	75.30	0.04	0.02	0.27
	7.60	460.00	400.00	4.42	36.18	0.24	4.26	146.25	42.51	0.15	0.02	0.22
	7.50	434.00	500.00	6.19	56.94	0.21	2.76	3.60	18.02	0.20	0.30	0.48
	7.30	396.60	613.10	6.67	25.06	0.35	8.14	128.37	366.38	0.00	0.01	0.10
	8.00	410.00	520.00	7.48	17.25	0.30	11.29	0.52	0.10	0.89	0.01	0.00
	8.10	379.00	576.00	2.89	23.73	0.39	13.11	0.35	2.29	0.42	8.08	5.98
	7.40	396.00	520.00	3.41	21.23	0.35	9.26	0.18	5.79	2.44	8.19	3.81
	7.50	150.00	384.00	6.37	27.01	0.30	6.79	0.20	15.10	0.51	8.61	5.62
	7.60	393.00	486.00	8.82	113.07	0.39	4.26	365.25	24.19	0.11	10.05	5.45
	7.50	418.00	335.00	0.95	35.59	0.20	8.65	32.64	2.16	0.69	2.34	7.24
	8.50	347.00	707.00	0.48	116.60	0.26	28.02	0.05	0.88	2.30	3.36	3.70
	7.60	402.30	364.50	5.54	35.25	0.20	6.25	0.21	0.01	3.31	4.16	5.00
	7.30	346.00	366.00	2.99	23.06	0.27	4.64	0.07	0.26	2.53	8.58	9.55
	7.50	334.00	353.00	1.17	18.27	0.25	3.06	11.50	0.69	3.41	8.84	7.71
	7.20	353.00	365.00	3.24	5.23	0.25	1.94	0.00	0.17	0.49	8.35	4.64
	8.10	374.00	691.00	1.67	21.30	0.13	2.33	2.29	0.35	0.42	8.08	5.98
	7.80	428.80	337.30	8.06	15.77	0.35	6.33	219.73	16.71	4.31	16.10	2.08
	7.50	373.00	523.00	6.06	48.55	0.24	4.84	4.00	0.78	1.50	5.05	2.87
	7.70	311.00	336.00	1.53	103.83	0.39	24.29	1.22	1.84	2.74	7.91	10.70
	7.60	401.00	531.00	5.42	78.83	0.21	7.87	25.64	0.24	2.45	3.13	3.37
	7.10	63.00	373.00	3.03	38.90	0.39	9.10	2.69	0.33	3.36	5.74	6.17
	7.90	364.00	585.00	5.42	78.83	0.21	7.87	25.64	0.24	2.45	3.13	3.37
	7.60	442.00	407.00	5.01	42.90	0.24	6.31	0.66	0.02	3.06	3.46	2.72
	7.60	398.00	344.00	5.86	99.19	0.26	8.12	1.66	0.01	2.04	5.38	4.84
	7.40	324.00	524.00	2.93	18.44	0.25	1.90	2.04	0.12	0.88	8.45	6.69
Min	**7.10**	**63.00**	**335.00**	**0.48**	**5.23**	**0.13**	**1.90**	**0.00**	**0.01**	**0.00**	**0.01**	**0.00**
Max	8.50	460.00	707.00	8.82	116.60	0.40	28.02	365.25	366.38	4.31	16.10	10.70
Median	**7.60**	**379.00**	**486.00**	**5.01**	**35.25**	**0.26**	**6.33**	**2.29**	**0.78**	**1.50**	**5.38**	**4.64**

Table S3: Details of isotopic measurements ($\delta^{238}U$, $^{234}U/^{238}U$ and U concentration) measured for the groundwater samples of this study.

	U	$\delta^{238}U$	$(^{234}U/^{238}U)$
	µg/L	‰	
Cluster 1			
	2.43	-0.23	1.87
	5.63	-0.35	1.57
	18.15	-0.40	1.59
	1.68	0.20	2.23
	7.24	-0.24	2.18
	11.56	-0.26	2.03
	5.69	-0.38	2.50
	5.99	-0.32	2.01
	20.18	-0.03	1.99
	24.66	-0.18	1.88
	48.25	0.08	1.53
	7.45	-0.15	2.34
	21.57	-0.14	1.91
	24.27	-0.15	2.27
	25.74	-0.16	2.27
	34.61	0.08	1.53
	8.35	0.33	2.08
	18.81	-0.05	1.64
	23.29	-0.30	2.18
Min	**1.68**	**-0.40**	**1.53**
Max	48.25	0.33	2.50
Median	**18.15**	**-0.16**	**2.01**
Cluster 2			
	7.7	-0.27	1.91
	20.51	-0.37	2.1
	5.04	-0.18	2.08
	8.99	-0.05	1.87
	14.72	-0.14	1.85
	7.2	-0.23	1.94
	27.15	-0.28	2.01
	40.23	0.16	1.82
	20.79	-0.08	2.05
	1.79	-0.38	1.59
	4.42	-0.33	1.93
	2.09	-0.5	2.27
	14.33	-0.23	2.21
	1.83	-0.19	1.97
	1.61	-0.07	1.96
	14.33	-0.46	2.14
Min	**1.61**	**-0.50**	**1.59**
Max	40.23	0.16	2.27
Median	**8.35**	**-0.23**	**1.97**
Cluster 3			
	8.87	0.01	1.96

12.64	0.22	2.09
5.48	0.00	1.99
7.66	0.06	2.05
12.59	-0.32	2.09
6.72	-0.2	2.08
6.47	-0.18	1.97
3.93	-0.2	1.95
6.33	-0.16	1.98
10.68	-0.21	2.25
7.78	-0.09	1.99
6.52	-0.18	1.81
2.12	-0.24	2.23
3.7	-0.34	1.59
2.12	0.9	2.1
15.88	0.33	2.42
0.45	-0.55	1.59
5.8	-0.26	1.92
5.35	-0.11	2.05
2.09	-0.11	2.07
7.74	-0.28	1.91
5.69	-0.18	1.89
6.7	0.41	2.36
6.69	-0.25	2.34
6.65	-0.29	2.08
6.48	-0.25	2.08
14.79	-0.07	2.03
5.07	-0.14	2.04
4.75	-0.15	1.95
5.52	-0.26	2.11
8.01	-0.18	1.96
5.11	-0.34	2.09
5.73	-0.21	2.03
13.58	-0.23	2.06
9.57	-0.05	1.7
4.19	-0.12	2.21
5.14	0.09	2.1
4.88	-0.23	2.24
6.74	-0.23	2.21
6.74	-0.19	1.97
5.85	-0.15	1.92
8.69	-0.24	2.05
4.91	-0.18	2.37
5.87	-0.14	2.26
4.77	-0.01	2.01
7.07	-0.07	1.96
8.24	-0.12	1.99
9.63	-0.28	2.24
7.8	-0.57	2.04
2.87	-0.34	2.06
4.71	-0.6	2.2
5.76	-0.27	2.09
7.44	-0.12	2.05
5.84	-0.11	1.98
5.63	-0.13	1.84

	11.05	-0.35	1.93
	6.78	-0.14	2.04
	4.63	-0.22	2.39
	2.37	-0.2	1.97
	4.43	-0.09	2.21
	8.95	-0.15	1.92
	8.24	-0.24	2.01
	5.5	-0.19	1.89
	11.24	-0.05	2.33
	5.39	-0.15	1.92
	4.56	-0.19	2.1
	6.15	-0.5	2.27
	6.9	-0.24	2.05
	4.51	-0.14	2.26
	5.99	-0.01	2.01
	7.21	-0.18	1.88
	5.8	-0.26	1.92
	13.81	0.36	2.12
	8.95	-0.18	1.92
	15.76	0.03	2.1
	9.62	-0.48	1.91
	3.96	-0.16	1.98
	4.13	-0.06	3.07
	8.69	-0.13	1.93
	3.3	-0.23	1.59
Min	**0.45**	**-0.60**	**1.59**
Max	15.88	0.90	3.07
Median	**6.24**	**-0.18**	**2.04**
Cluster 4			
	18.96	-0.07	1.8
	20.82	-0.27	2.03
	20.06	-0.24	1.94
	24.83	-0.18	1.7
	23.63	0.02	1.55
	48.25	-0.23	1.53
	45.11	-0.27	1.59
	9.68	-0.22	2.13
	31.02	0.07	1.62
	18.49	-0.2	2.13
	16.35	-0.37	1.83
	20.23	-0.19	2.1
	15.53	-0.21	2.05
	8.73	-0.32	1.94
	5.5	-0.68	1.54
	20.51	-0.24	2.14
	18.15	-0.12	1.76
	15.88	-0.22	2.12
	13.41	-0.3	1.83
	26.62	-1.06	2.06
	7.8	-0.26	2.04
	26.62	-0.29	2.05
	19.31	-0.32	2.01
	23.97	-0.18	2.37

	12.59	-0.32	2.09
Min	**5.50**	**-1.06**	**1.53**
Max	48.25	0.07	2.37
Median	**19.31**	**-0.24**	**2.01**

Table S4: U Species calculation using Geochemist Workbench

U Aqueous Species	Molality	% in total U species
$Ca_2UO_2(CO_3)_3(aq)$	2.69E-08	61.3%
$CaUO_2(CO_3)_3^{2-}$	1.48E-08	33.7%
$UO_2(CO_3)_2^{2-}$	8.59E-10	2.0%
$U(OH)_4(aq)$	7.10E-10	1.6%
$UO_2(CO_3)_3^{3-}$	2.38E-10	0.5%
$UO_2CO_3(aq)$	2.17E-10	0.5%
$UO_2(OH)_2(aq)$	1.56E-10	0.4%
$UO_2(OH)^+$	2.21E-12	0.0%
$UO_2(OH)_3^-$	1.75E-13	0.0%
$(UO_2)_2(OH)_3^-$	1.07E-13	0.0%
UO_2^{++}	5.60E-14	0.0%
$UO_2SO_4(aq)$	4.07E-15	0.0%
Sum	4.39E-08	100%

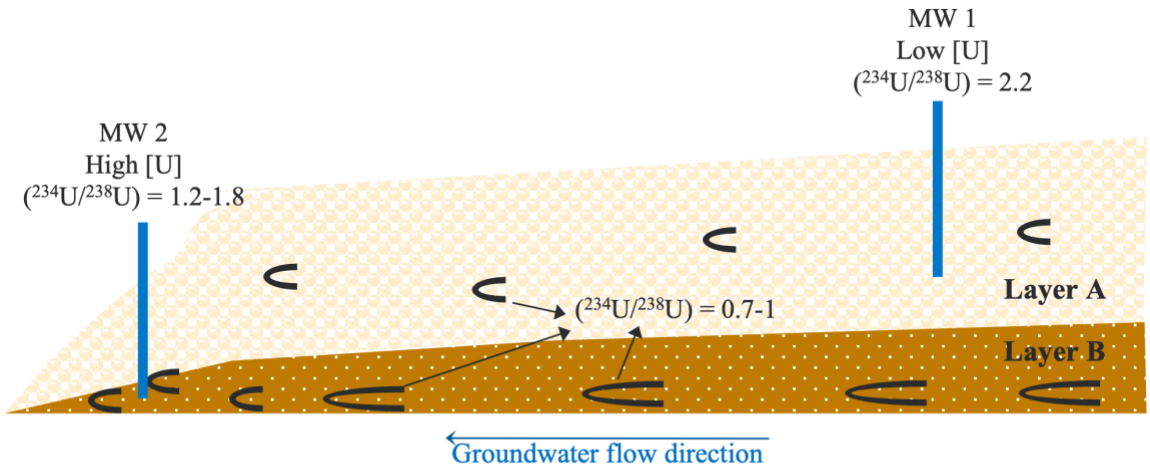

Layer A : Heterogeneously distributed U rich zones in sedimentary formation
Layer B: Ore grade U deposits in the basal part of the sedimentary formation

Figure S1: Conceptual diagram showing variation of ($^{234}U/^{238}U$) indicating proximity of the groundwater to a U source as well as variation due to groundwater transport process.

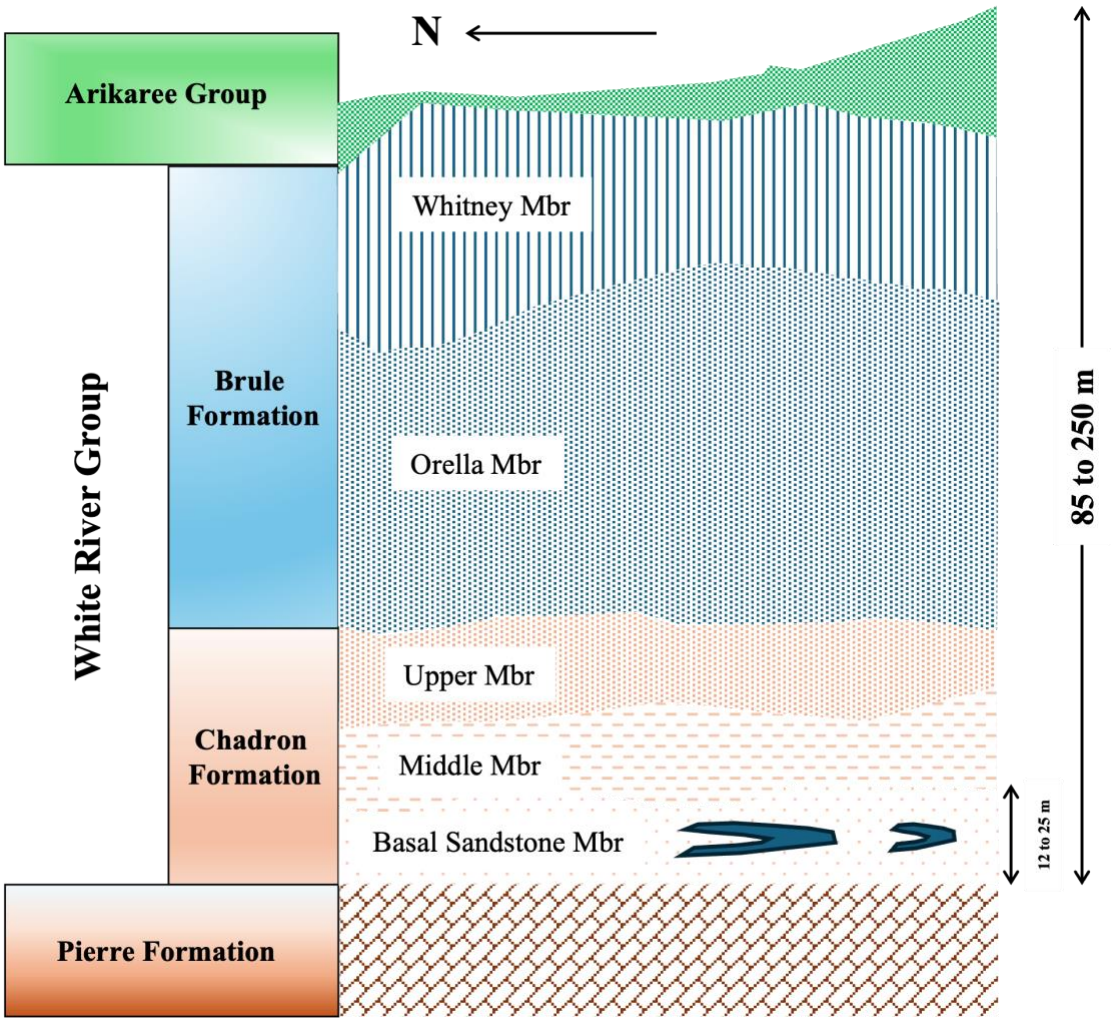

Figure S2: Schematic N-S lithostratigraphic section across the study area. Note that the U-hosting basal Chadron sandstone member contains more than two stacked ore rolls.

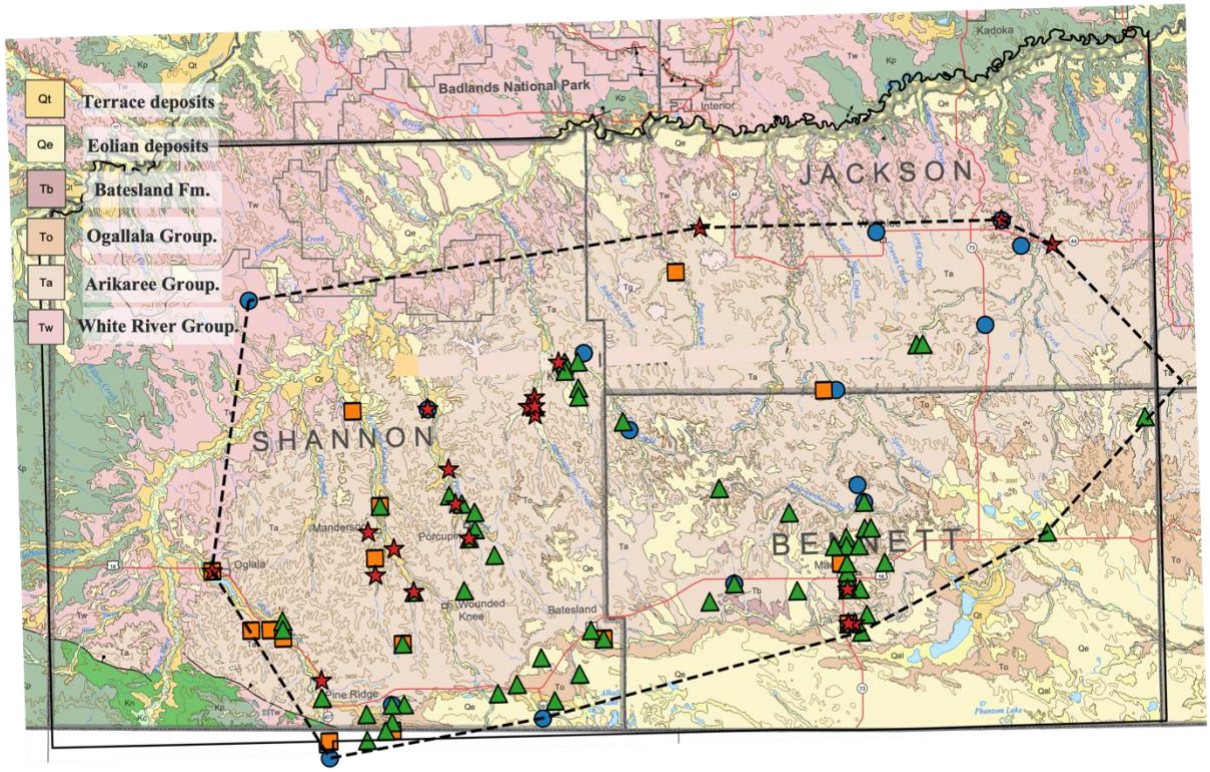

Figure S3: Map showing the geological units of our study area with sample locations (n=141) with cluster information on them. The geological units are traced from Martin et. al., 2004[101]

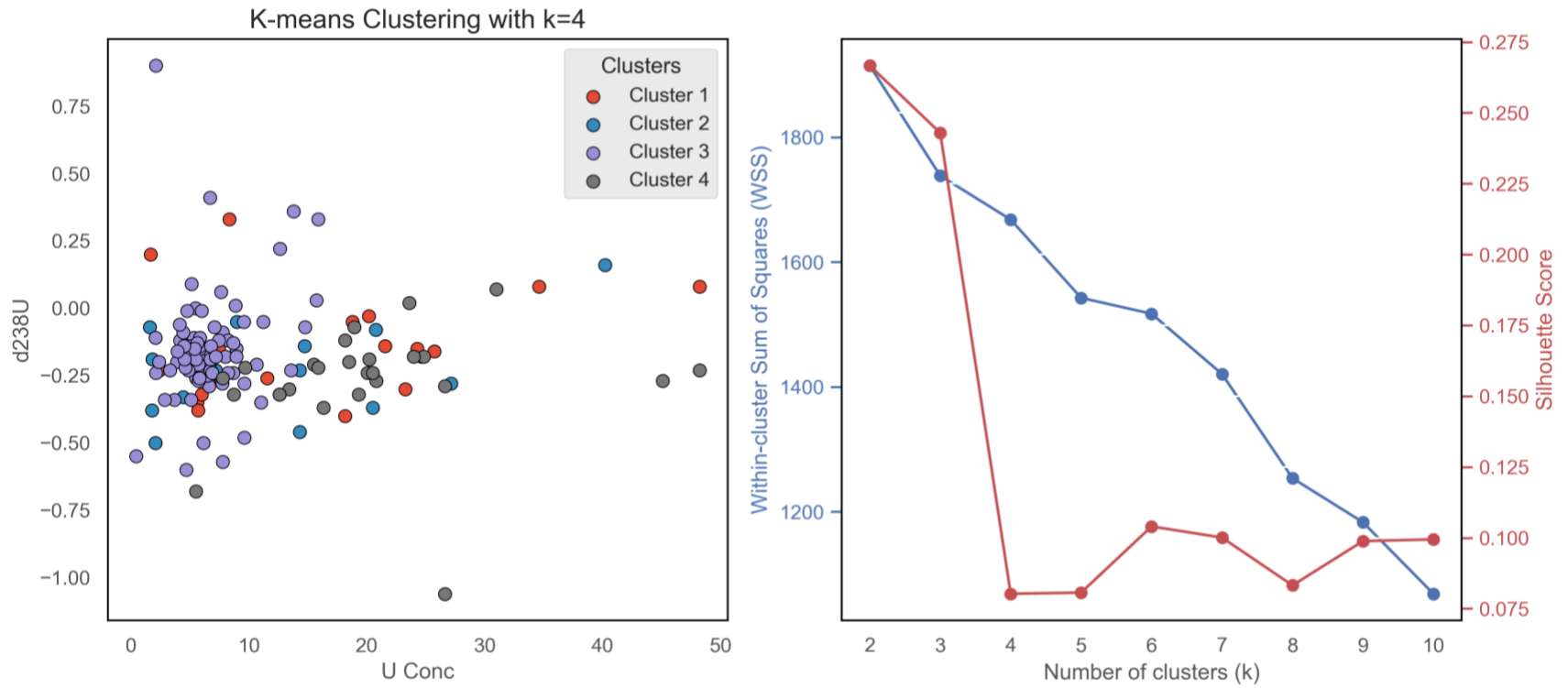

Figure S4: Figure: K-means clustering results and cluster evaluation metrics. (Left) Scatter plot of K-means clustering with *k=4*, showing the distribution of data points based on uranium concentration (U Conc) and $\delta^{238}U$ values. Different colors represent distinct clusters. (Right) Evaluation of clustering performance using the elbow method (blue line) and silhouette score (red line). The within-cluster sum of squares (WSS) decreases as the number of clusters increases, indicating improved compactness, while the silhouette score

helps assess cluster separation, peaking around *k=.4*

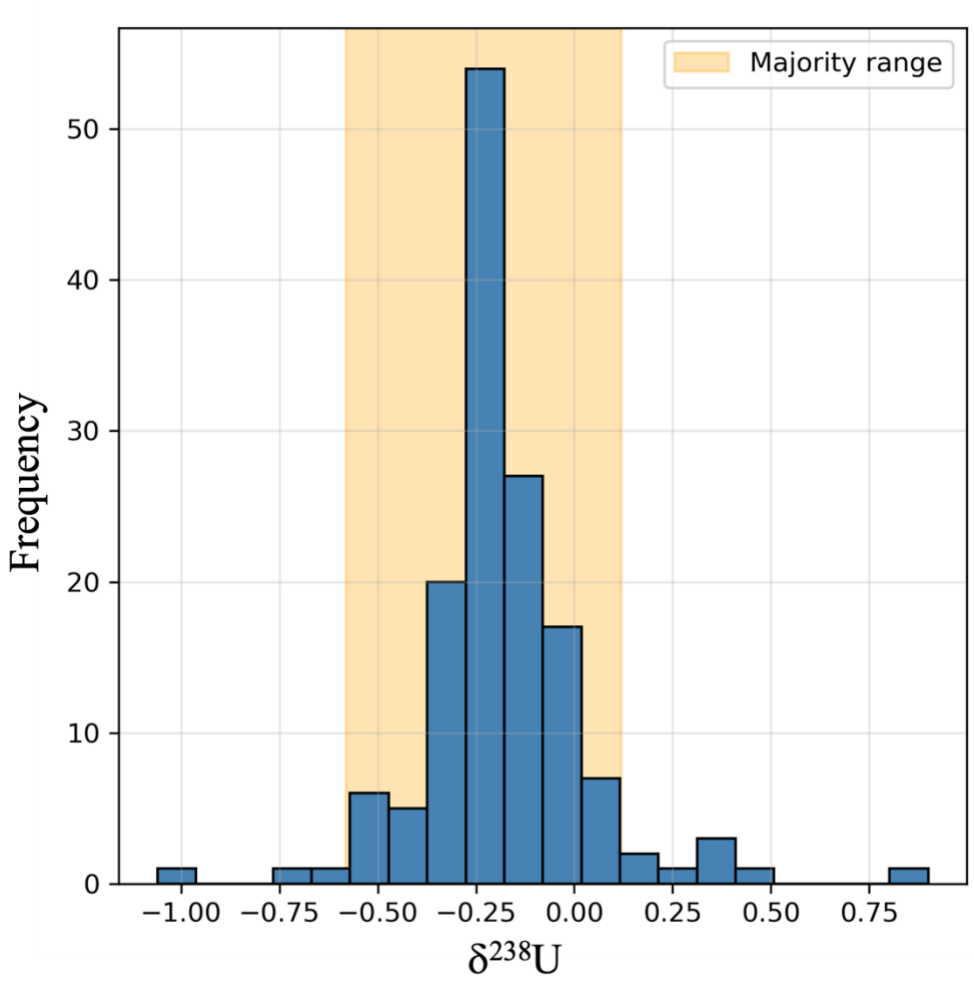

Figure S5: Histogram of our groundwater $\delta^{238}U$ showing its major distribution in this study.

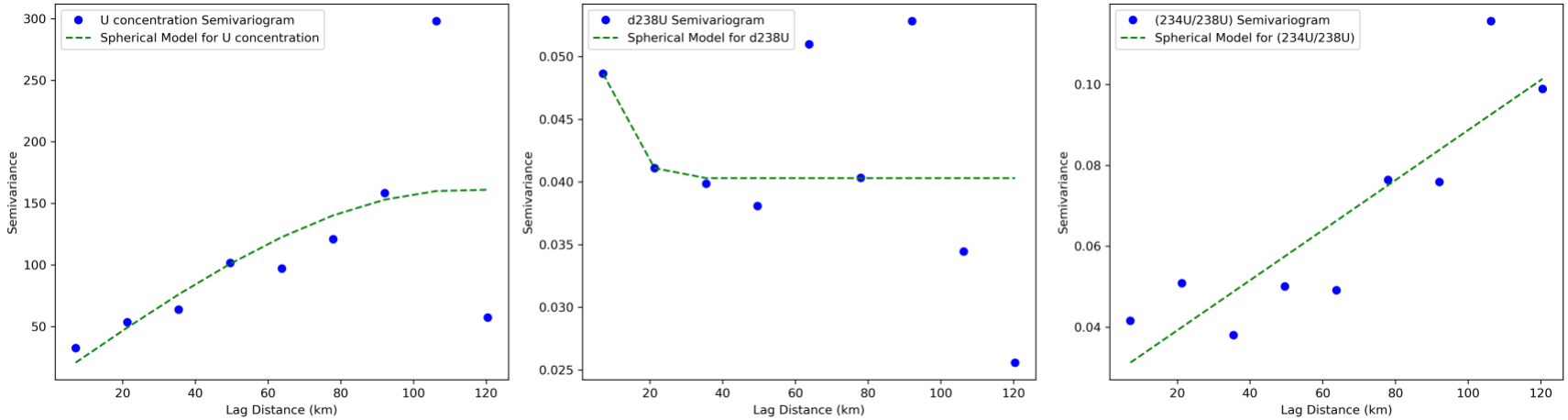

Figure S7: Semivariogram of U concentration, $\delta^{238}U$ and ($^{234}U/^{238}U$

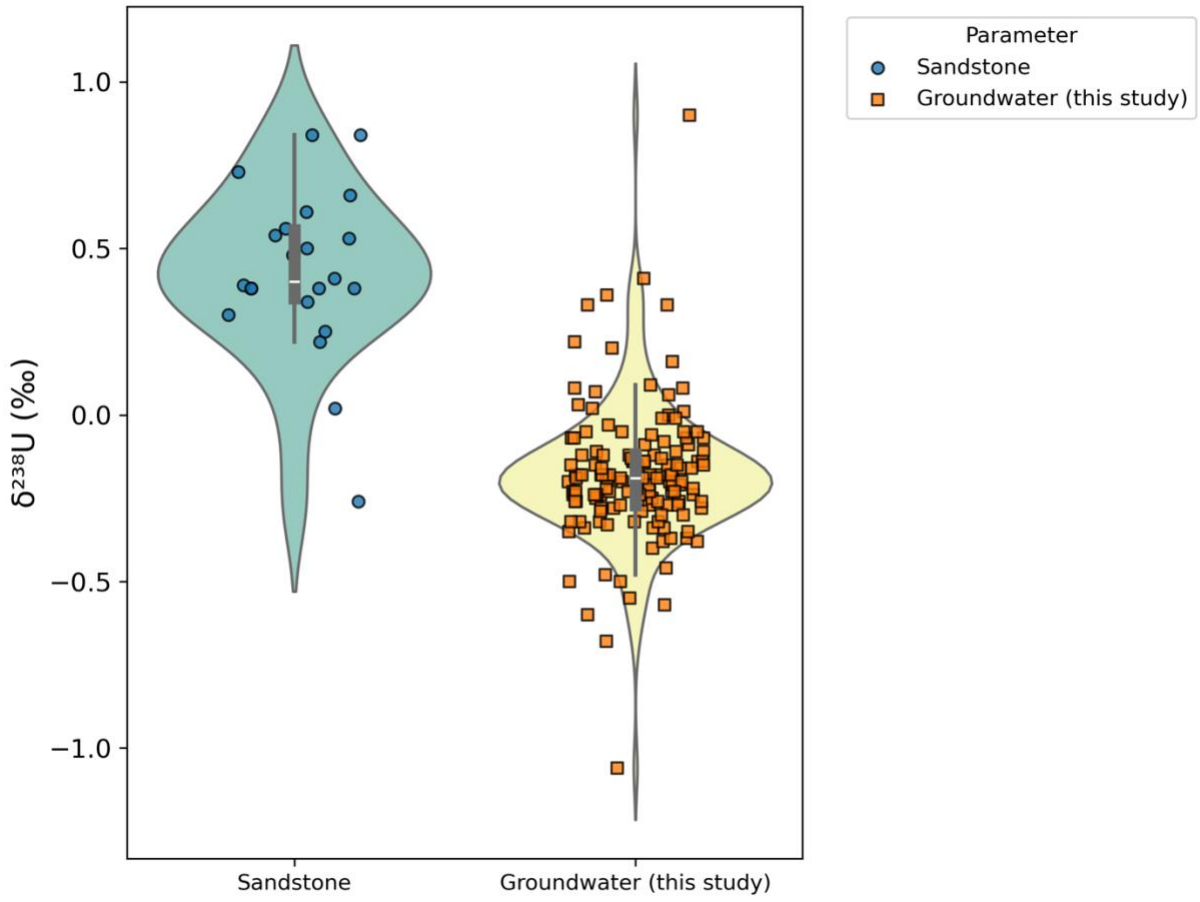

Figure S7: Violin plot showing distribution and variability of $\delta^{238}U$ within the groundwater and sandstone hosted U deposit terrain, showing the full range and frequency of values. The blue circles are literature for sandstone and orange square is for sample data used to create this plot. The data for sandstone type deposit are sourced from these references. [75–77]

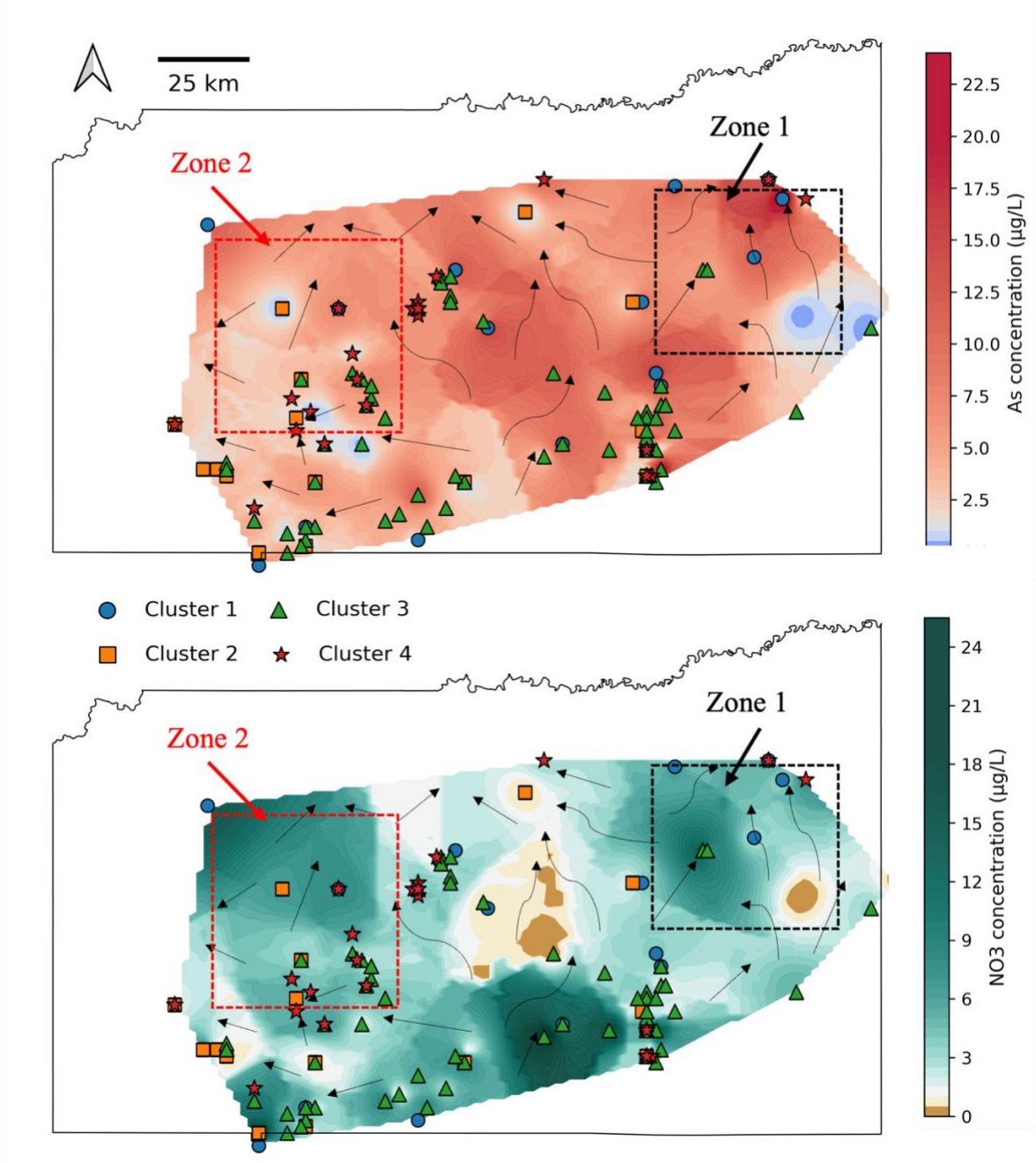

Figure S8: Spatial distribution of nitrate (NO_3^-) levels with groundwater flow direction. The unit of NO_3^-concentration is mg/L

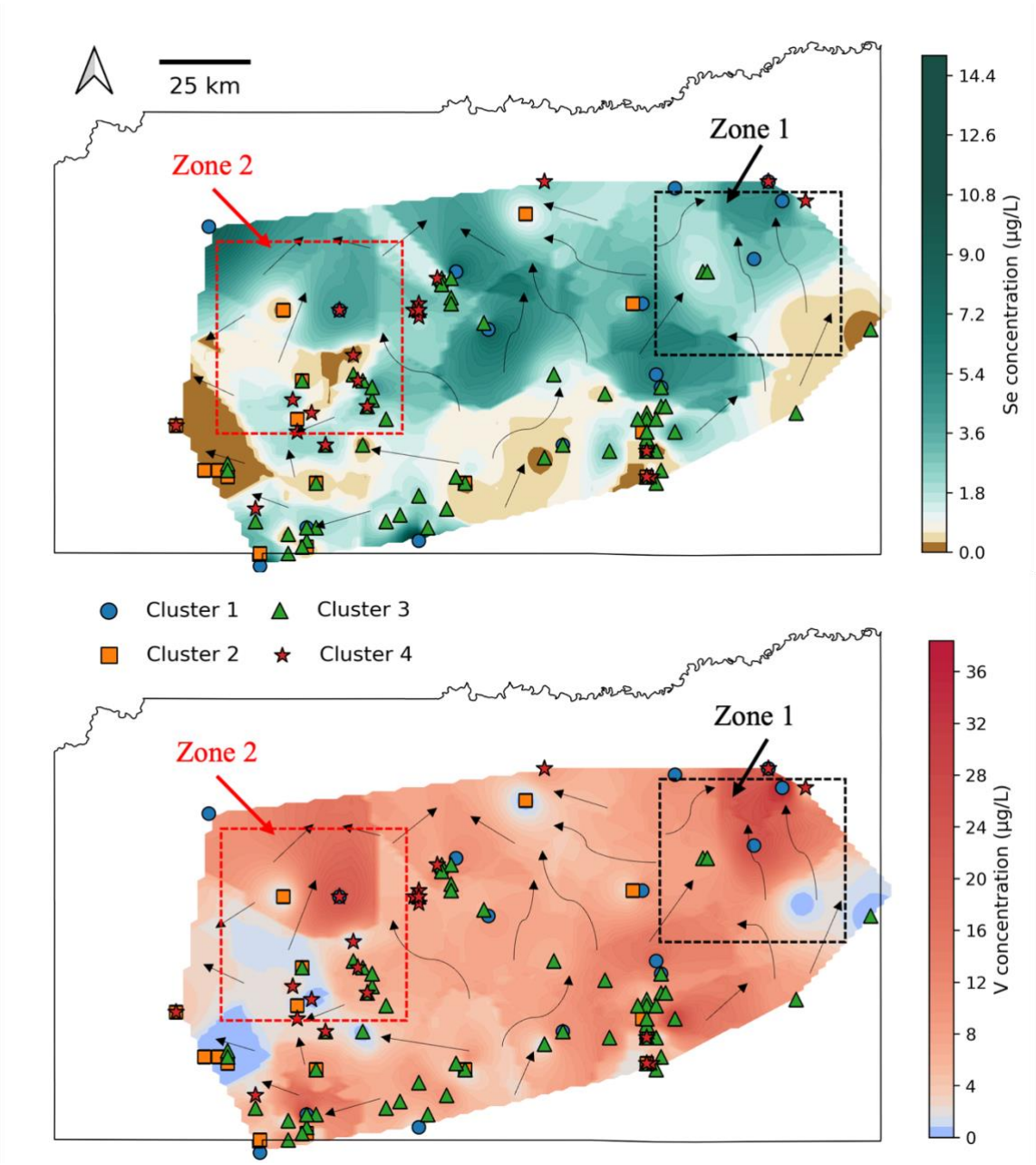

Figure S9: Spatial distribution of selenium (Se) and vanadium (V) levels with groundwater flow direction.

The unit of Se and V concentration is µg/L

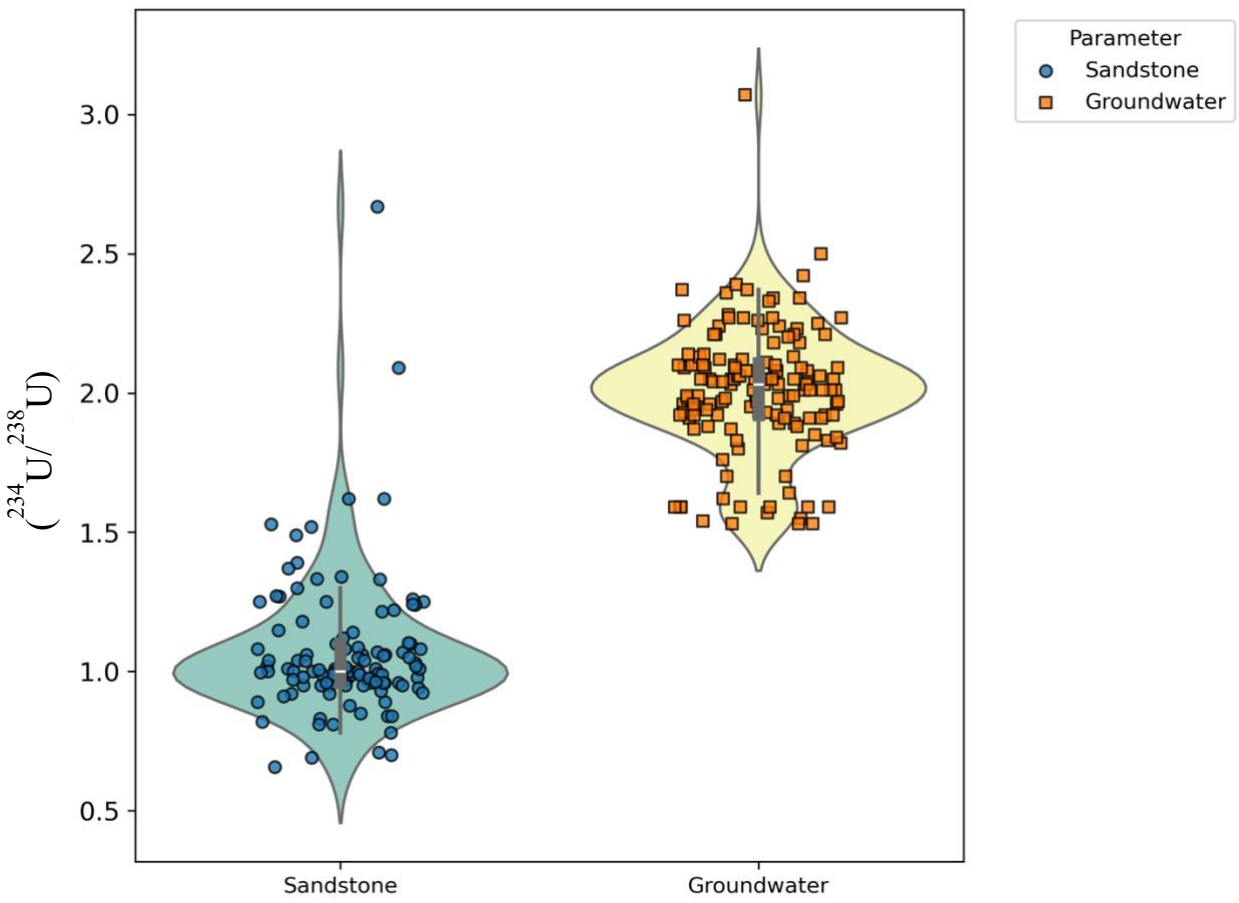

Figure S10: Violin plot showing distribution and variability of ($^{234}U/^{238}U$) within the groundwater and sandstone hosted U deposit terrain, showing the full range and frequency of values. The blue circles are literature for sandstone and orange square is for sample data used to create this plot. The data for sandstone type deposit are sourced from these references. [31,89–91]

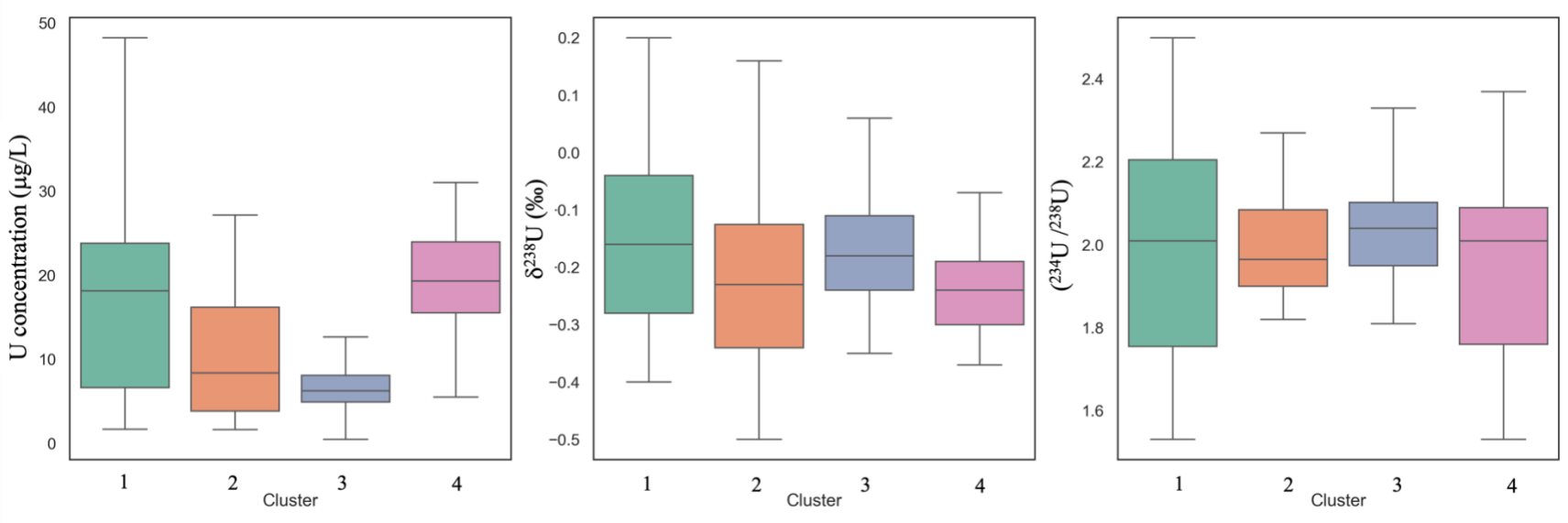

Figure S11: Box plots showing distribution of $\delta^{238}U$, ($^{234}U/^{238}U$) and U concentration for the three clusters (1-4). Lower and upper box boundaries are 25th and 75th percentiles, black bold line inside the box indicate the median. Lower and upper error lines are for 10th and 90th percentiles. Black bold line on the top of box plots denotes p-values showing statistical significance between each cluster. The p-values represent the results of pairwise comparisons, highlighting significant differences ($p < 0.05$) between the clusters, with lower p-values indicating stronger statistical distinction. Outliers from the U concentration are removed from this plot to show the variation in different clusters. They are listed in Table S2.

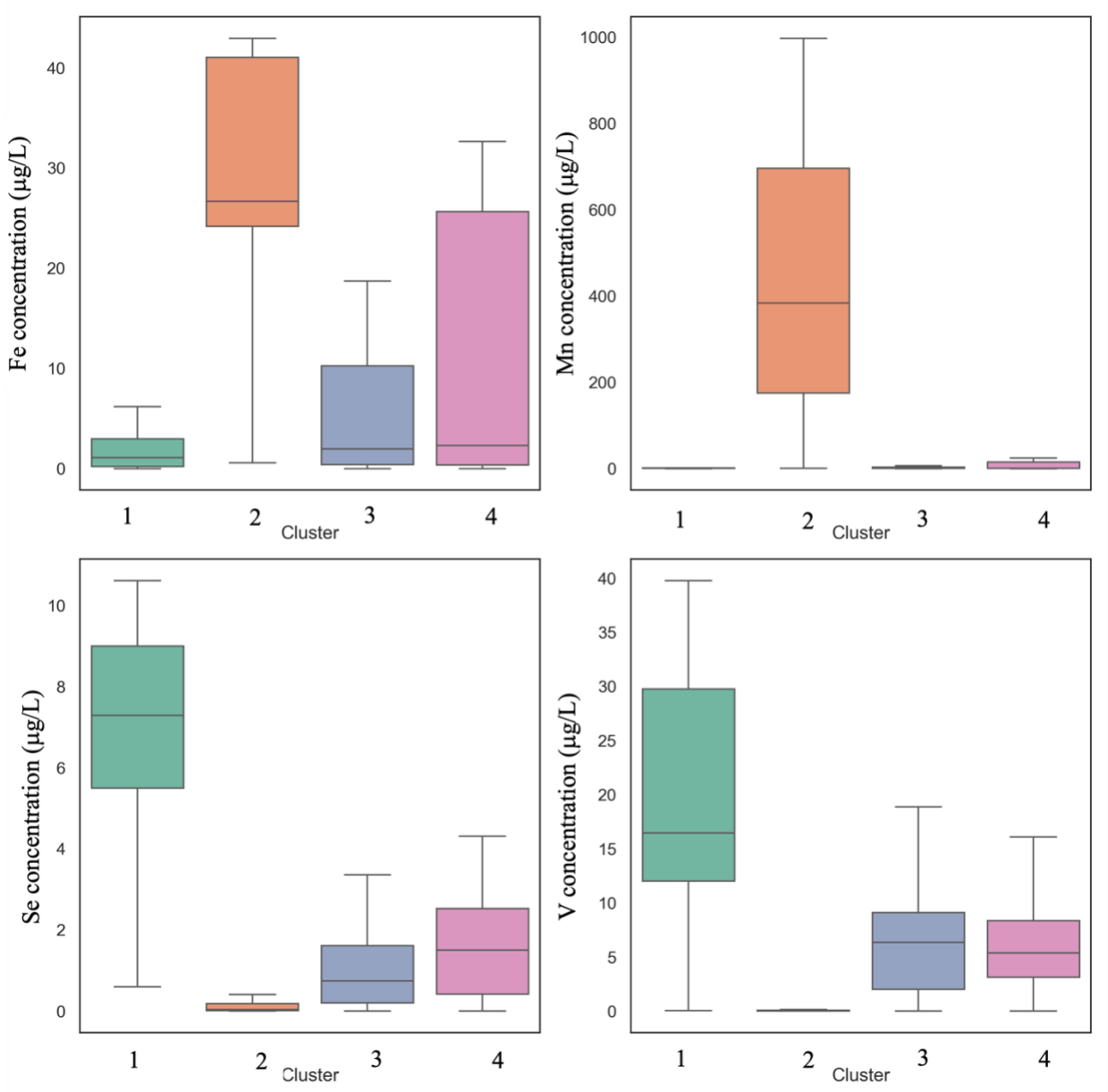

Figure S12: Box plots showing distribution of redox sensitive elements: Fe, Mn, Se and V concentration for the four clusters (1-4). Lower and upper box boundaries are 25th and 75th percentiles, black bold line inside the box indicate the median. Lower and upper error lines are for 10th and 90th percentiles. Black bold line on the top of box plots denotes p-values showing statistical significance between each cluster. The p-values represent the results of pairwise comparisons, highlighting significant differences ($p < 0.05$) between the clusters, with lower p-values indicating stronger statistical distinction. Outliers are removed from this plot to show the variation in different clusters. They are listed in Table S1.

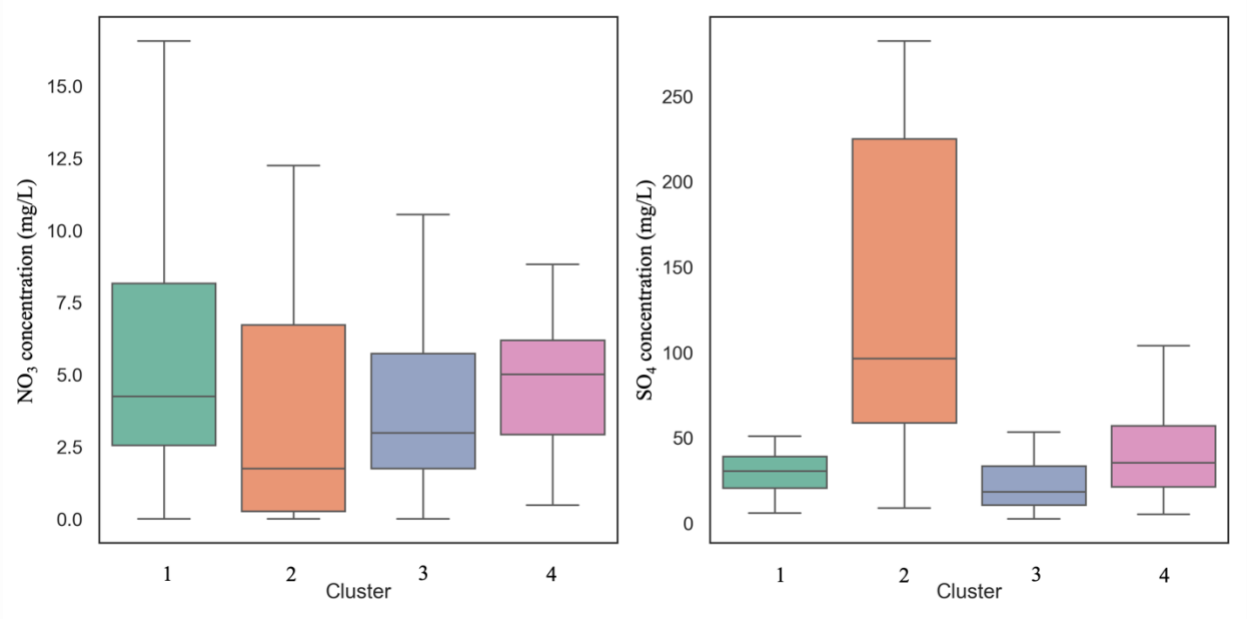

Figure S13: Box plots showing distribution of major anions: NO_3^- and SO_4^{2-}concentration for the four clusters (1-4). Lower and upper box boundaries are 25th and 75th percentiles, black bold line inside the box indicate the median. Lower and upper error lines are for 10th and 90th percentiles. Black bold line on the top of box plots denotes p-values showing statistical significance between each cluster. The p-values represent the results of pairwise comparisons, highlighting significant differences ($p < 0.05$) between the clusters, with lower p-values indicating stronger statistical distinction. Outliers are removed from this plot to show the variation in different clusters. They are listed in Table S1.

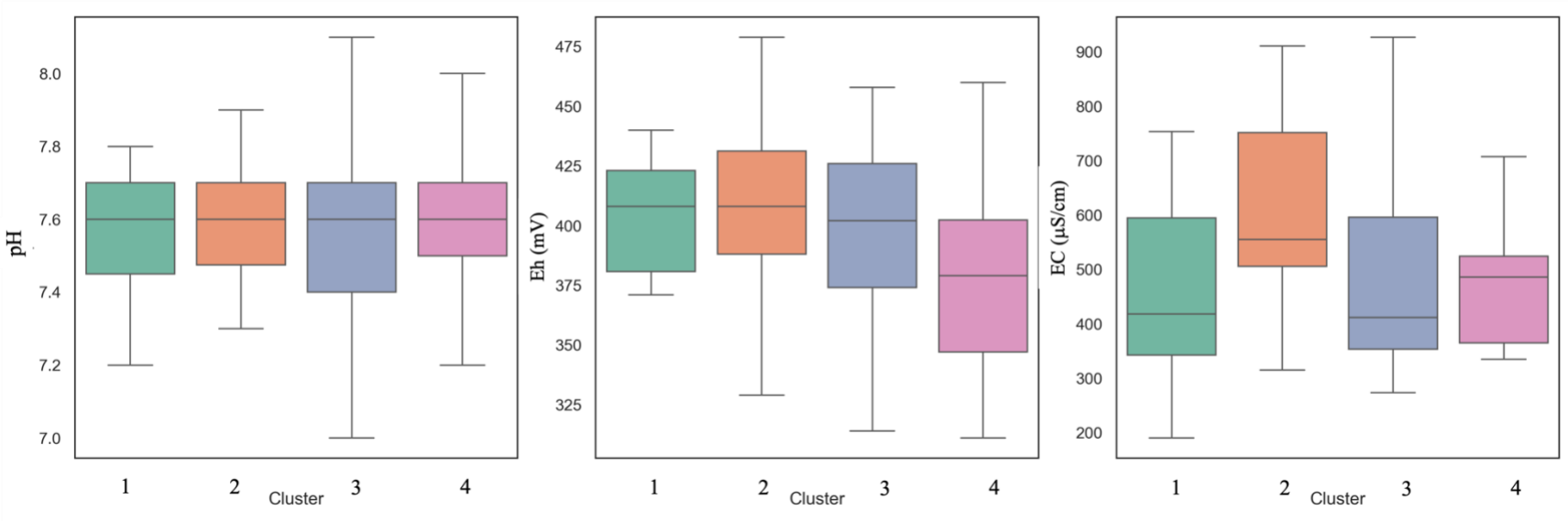

Figure S14: Box plots showing distribution of field paramters: pH, Eh (mV) and EC (mS/cm) concentration for the four clusters (1-4). Lower and upper box boundaries are 25th and 75th percentiles, black bold line inside the box indicate the median. Lower and upper error lines are for 10th and 90th percentiles. Black bold line on the top of box plots denotes p-values showing statistical significance between each cluster. The p-values represent the results of pairwise comparisons, highlighting significant differences ($p < 0.05$) between the clusters, with lower p-values indicating stronger statistical distinction. Outliers are removed from this plot to show the variation in different clusters. They are listed in Table S1.

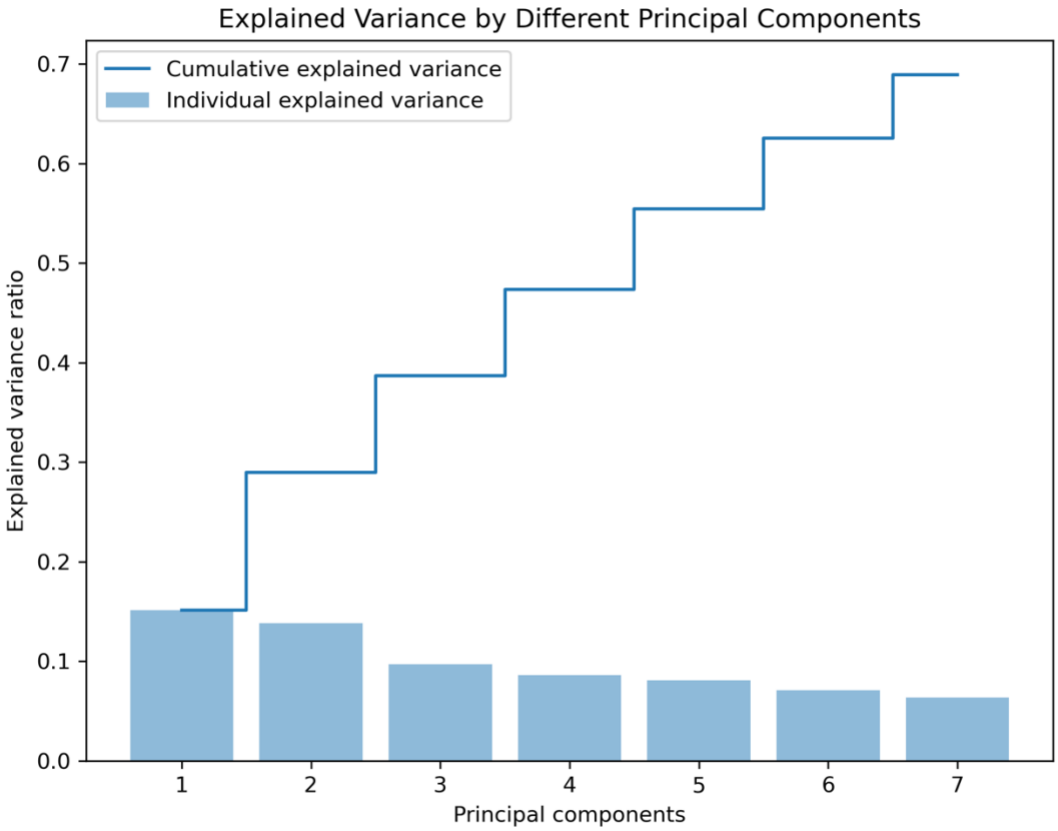

Figure S15: Explained Variance by Different Principal Components. The bar plot represents the individual explained variance ratio for the seven principal components, while the line plot shows the cumulative explained variance. The cumulative variance reaches approximately 70%, highlighting the contribution of the principal components in capturing the variability in the dataset.